Food & Function

Accepted Manuscript

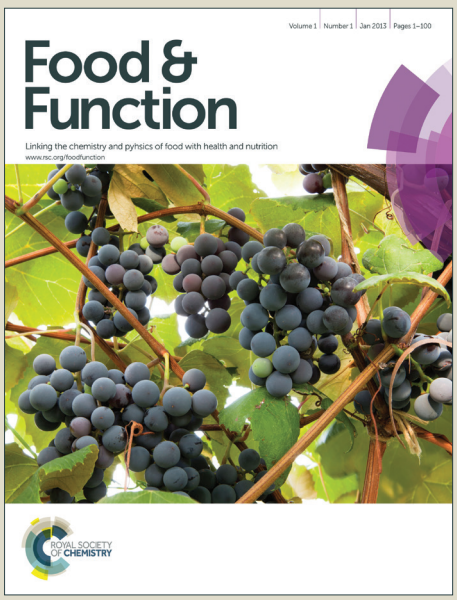

This is an *Accepted Manuscript*, which has been through the Royal Society of Chemistry peer review process and has been accepted for publication.

Accepted Manuscripts are published online shortly after acceptance, before technical editing, formatting and proof reading. Using this free service, authors can make their results available to the community, in citable form, before we publish the edited article. We will replace this *Accepted Manuscript* with the edited and formatted *Advance Article* as soon as it is available.

You can find more information about *Accepted Manuscripts* in the Information for Authors.

Please note that technical editing may introduce minor changes to the text and/or graphics, which may alter content. The journal's standard Terms & Conditions and the Ethical guidelines still apply. In no event shall the Royal Society of Chemistry be held responsible for any errors or omissions in this *Accepted Manuscript* or any consequences arising from the use of any information it contains.

ROYAL SOCIETY OF CHEMISTRY

www.rsc.org/foodfunction

Reactivity of food phenols with iron and copper ions: binding, dioxygen activation and oxidation mechanisms

Ezzohra Nkhili,[a] Michèle Loonis,[b] Simona Mihai,[c] Hakima El Hajji,[a] and Olivier Dangles*[c]

[a] *University Cadi Ayyad, Marrakech, Morocco*

[b] *INRA, UMR408, F-84000 Avignon, France*

[c] *University of Avignon, UMR408, F-84000 Avignon, France*

E-mail: olivier.dangles@univ-avignon.fr

Fax: (+33) 490 14 44 41; Tel: (+33) 490 14 44 46

Food & Function Accepted Manuscript

Abstract

In this work, the affinity of common dietary phenols (gallic acid, caffeic acid, catechin, rutin) for iron and copper ions was quantitatively investigated in neutral phosphate buffer as well as the reactivity of the complexes toward dioxygen. Contrasted behaviors were observed: because of the competing phosphate ions, Fe^{III} binding is much slower than Fe^{II} binding, which is rapidly followed by autoxidation of Fe^{II} into Fe^{III}. With both ions, O_2 consumption and H_2O_2 production are modest and the phenolic ligands are only slowly oxidized. By contrast, metal – phenol binding is fast with both Cu^{I} and Cu^{II}. With Cu^{I}, O_2 consumption and H_2O_2 production are very significant and the phenolic ligands are rapidly oxidized into a complex mixture of oligomers. The corresponding mechanism with Cu^{II} is hampered by the preliminary rate-determining step of Cu^{II} reduction by the phenols. The consequences of these findings for the stability and antioxidant activity of plant phenols are discussed.

Keywords: polyphenol, gallic acid, caffeic acid, catechin, rutin, iron, copper, binding, oxidation

Food & Function Accepted Manuscript

1 Introduction

Plant phenols, such as simple hydroxylated derivatives of benzoic and cinnamic acids and the more complex polyphenols (flavonoids, tannins), are ubiquitous in food and consumed in substantial concentrations.[1-3] Plant phenols typically have a favorable impact on food quality, *e.g.* by acting as antioxidants for the preservation of polyunsaturated lipids,[4] by expressing or stabilizing natural colors[5] and by providing the adequate astringency to wines owing to their affinity for salivary proteins.[6] In addition, plant phenols are usually regarded as beneficial to human health,[7] in particular by preventing the development of degenerative diseases (type 2 diabetes and cardiovascular disease, possibly some cancers and age-related disorders). Although the clinical demonstration of these protective effects at low nutritional doses and over extended periods of time is quite difficult to provide,[8] the wealth of *in vitro* and *in vivo* studies on that matter strongly suggests that dietary plant phenols help fight degenerative diseases by a combination of their antioxidant activity (in particular, in the upper digestive tract)[9] and more specific biological effects (*e.g.*, anti-inflammatory)[10] reflecting the affinity of plant phenols and their human metabolites for specific cell proteins. Overall, it is desirable to maintain a high phenolic content in plant food during industrial processing, storage and cooking and also to better understand the mechanisms underlying their degradation and the expression of their potential health effects.

Iron and copper ions are present in substantial concentrations in food,[11] usually bound to plant or animal proteins. Beside radiations, these transition metal ions are the most likely inducers of oxidative processes that may alter electron-rich micronutrients such as phenols[12] and carotenoids.[13] Iron and copper ions (either loosely bound or at the active site of metalloproteins) are also typically required in the formation of the reactive oxygen species (ROS) involved in oxidative stress and in the initiation of polyunsaturated lipid oxidation.[14] Interestingly, many common dietary phenols display a catechol (1,2-dihydroxybenzene) nucleus that confers on them both an affinity for metal ions (although keto groups with nearby hydroxyl groups can also contribute in many flavonoids) and an electron-donating capacity usually associated with a potent antioxidant activity.[9] Thus, catechol-containing plant phenols can express a rich, although still incompletely known, chemistry with iron and copper ions combining binding and redox processes.[15]

Up to now, several studies have been published on metal - plant phenol complexes (determination of binding constants and binding sites)[16,17] and on the ability of plant phenols to modulate the redox status of iron and copper[12,18-21] and the Fenton reaction.[17,22] Indeed, metal-polyphenol interactions are expected to interfere with the ROS-forming process, either in an

Food & Function Accepted Manuscript

inhibitory / antioxidant way via the formation of inert metal complexes, or in a stimulatory / pro-oxidant way.[22] In the latter situation, polyphenols act as electron donors to metal ions for the reduction of H_2O_2 into $HO^{\bullet}$ (Fenton reaction).

Based on H_2O_2 production and rate constants for the consumption of the metal complexes, copper ions are much more efficient than iron ions at promoting electron transfers from the flavonol quercetin to O_2 in neutral conditions.[12,17] The influence of the flavanol dimer procyanidin B2 on the H_2O_2-induced cleavage of DNA also provides an interesting example of the discriminated reactivity of polyphenols with copper and iron ions. Indeed, procyanidin B2 reduces Cu^{II} into Cu^{I}, which forms hydroperoxo complexes with H_2O_2 that can cleave DNA (pro-oxidant activity). By contrast, procyanidin B2 forms with Fe^{II} a complex that is inert in the Fenton reaction (antioxidant activity).[23] A similar study with a larger set of plant phenols confirmed that phenols were less effective at inhibiting DNA damage induced by Cu^{I} - H_2O_2 (some being even pro-oxidant) than the corresponding process with Fe^{II}.[24]

The kinetics of metal – polyphenol binding and subsequent reactions of the complexes with O_2 as well as the corresponding mechanisms are relatively poorly documented despite the importance of the topic for interpreting the chemical stability of plant phenols and their pro- or antioxidant activity in food and in humans. These points are specifically addressed in this work with a selection of 4 common dietary phenols (Scheme 1).

2 Experimental section

All experiments were conducted in a 0.01 M phosphate buffer (pH 7.4).

2.1 Chemicals

Rutin dihydrate (95%), caffeic acid, catechin, gallic acid, $FeSO_4$, $7H_2O$ (99%), $Fe(NO_3)_3$, $6H_2O$ (99.9%), $CuCl_2$, $2H_2O$ (99.9%), CuCl (99+%), xylenol orange sodium salt, ferrozine (5,6-diphenyl-3-(2-pyridyl)-1,2,4-triazine-4',4''-disulfonic acid sodium salt hydrate, 97%), bathocuproin disulfonic acid disodium salt hydrate, BHT (butylated hydroxytoluene) and H_2O_2 (30%) were from Sigma-Aldrich.

2.2 Analyses

Food & Function Accepted Manuscript

Complexation and autoxidation reactions. The complexation and autoxidation processes were monitored using a HP 8453 diode-array spectrometer equipped with a magnetically stirred quartz cell (optical pathlength: 1 cm). The temperature in the cell was kept at 37°C by means of a thermostated bath. The $5x10^{-3}$ M solutions of metal ion were prepared in MeOH (Fe^{III}, Cu^{II}) or MeOH-0.2 M H_2SO_4 96:4 (Fe^{II}) or MeCN-0.2 M HCl 96:4 (Cu^{I}). The Fe^{II} and Cu^{I} solutions were prepared daily and checked for autoxidation using the proper colorimetric tests (see below).

To 2 ml of the pH 7.4 buffer solution (10^{-2} M phosphate) placed in the spectrometer cell were successively added 20 µl of a freshly prepared $5x10^{-3}$ M solution of phenol in MeOH and 10-100 µl of a freshly prepared $5x10^{-3}$ M solution of metal ion. Spectra were recorded every 0.5 s over 2 min (complexation) and every 30 s over 120 min (autoxidation).

H_2O_2 Titration.[25] The FOX2 reagent was prepared by mixing a solution of xylenol orange sodium salt (38 mg) and BHT (440 mg) in MeOH (450 ml) with a solution of $FeSO_4$, $7H_2O$ (49 mg) in 50 ml of 0.25 M H_2SO_4. Hence, the final composition of the FOX2 reagent was: 10^{-4} M xylenol orange, $4x10^{-3}$ M BHT, $25x10^{-3}$ M H_2SO_4 and $25x10^{-5}$ M $FeSO_4$, $7H_2O$ in 90% (v/v) MeOH. Aliquots (0.5 ml) of a 10^{-4} M solution of phenol (phosphate pH 7.4, 37°C) in the presence or absence of metal ion (1 equiv.) were rapidly taken up, diluted into 1.5 ml of FOX2 reagent at room temperature, and stirred for 10 min. The samples were then transferred to the spectrometer cell for recording the absorbance at 592 nm (λ_{max} of the Fe^{III}-xylenol orange complex). In control experiments without phenol, addition of Fe^{III}, Cu^{II} or Cu^{I} to the FOX2 reagent caused a time-dependent increase in A(592 nm) (attributed to slow metal exchange on the xylenol orange ligand) whose amplitude is in the order $Fe^{III} > Cu^{II} > Cu^{I}$. The corresponding values must be subtracted. Corrections using Fe^{III} apply to any experiment involving iron ions, since Fe^{II} is rapidly autoxidized to Fe^{III} in the pH 7.4 phosphate buffer. Corrections using Cu^{I} apply to experiments using the phenols and Cu^{I} or Cu^{II}, since the latter is rapidly reduced to Cu^{I} by the phenols. Since distinct values are obtained for corrections with Cu^{I} and Cu^{II}, it is assumed that Cu^{I} autoxidation is negligible in the presence of the FOX2 reagent (Cu^{I} rapidly added to a FOX2 reagent-phosphate buffer (3:1) mixture). The H_2O_2 concentration is deduced from a calibration curve constructed by mixing the FOX2 reagent (1.5 ml) with aliquots (0.5 ml) of aqueous H_2O_2 solutions of known concentrations obtained by dilution of a 0.01 M solution (concentration determined from $\varepsilon(H_2O_2)$ = 40 M^{-1} cm^{-1} at 240 nm). In those conditions, the apparent ε value of the Fe^{III}-xylenol orange complex at 592 nm was $65x10^{3}$ M^{-1} cm^{-1}.

Fe^{II} Titration.[26] Aliquots (0.5 ml) of a 10^{-4} M solution of phenol (phosphate pH 7.4, 37°C) in the presence of Fe^{II} or Fe^{III} (1 equiv.) were rapidly taken up, diluted into 1.5 ml of a 10^{-3} M

Food & Function Accepted Manuscript

ferrozine solution at room temperature, and stirred for 10 min. The samples were then transferred to the spectrometer cell for recording the absorbance at 564 nm (λ_{max} of the Fe^{II}-ferrozine complex, $\varepsilon = 27900\ M^{-1}\ cm^{-1}$).

Cu^{I} Titration.[27] Aliquots (0.5 ml) of a 10^{-4} M solution of phenol (phosphate pH 7.4, 37°C) in the presence of Cu^{II} or Cu^{I} (1 equiv.) were rapidly taken up, diluted into 1.5 ml of an aqueous 10^{-3} M solution of bathocuproin disulfonate at room temperature, and stirred for 10 min. The samples were then transferred to the spectrometer cell for recording the absorbance at 480 nm (λ_{max} of the Cu^{I}-bathocuproin disulfonate complex, $\varepsilon = 13900\ M^{-1}\ cm^{-1}$).

HPLC-MS. Analyses were performed on a HP 1050 model equipped with a diode-array detector and coupled to a Micromass LCZ 4000 mass spectrometer. A C_{18} column (4.6x150 mm, 5 µm particle size) equipped with a pre-column (4.6x7.5 mm, 5 µm particle size) and kept at 25°C was used. The mobile phase (flow rate: 1.0 ml min^{-1}) was a linear gradient of MeCN and 0.05% aqueous HCO_2H with 5% MeCN at time 0 and 100% MeCN at 60 min. Mass spectra were recorded in the negative electrospray mode.

Ultra-fast HPLC-MS. Analyses were performed on a Waters Acquity™ Ultra Performance LC® system equipped with a Waters diode array detector and coupled to a Bruker-daltonics HCT ultra ion trap MS. A Waters acquity™ reversed-phase C_{18} column type BEH (2.1x50 mm, 1.7 µm particle size) kept at 35°C was used. The mobile phase (flow rate: 0.28 ml min^{-1}) was a gradient of MeOH and 0.05% aqueous HCO_2H with 5% MeOH at time 0 and 100% MeOH at 10 min. Mass spectra were recorded in the negative electrospray mode.

Dioxygen consumption. Analyses were carried out with help of an optic fiber probe (oxygen Microoptode, PreSens) directly inserted into the magnetically stirred solution. The O_2 concentration was recorded by the Microx TX3 oxygen meter (PreSens).

Data Analysis. The curve-fittings of the absorbance *vs*. time plots were carried out on a PC using the Scientist program (MicroMath, Salt Lake City, USA). Beer's law and sets of differential kinetic equations (see text for the kinetic models used) with initial conditions on concentrations were input in the model. Curve-fittings were achieved through least square regression and yielded optimized values for the parameters (kinetic rate constants, molar absorption coefficients, stoichiometries). Standard deviations are reported.

Food & Function Accepted Manuscript

3 Results

Gallic acid (GA), caffeic acid (CA), catechin and rutin (quercetin 3-O-β-rutinoside) (Scheme 1) were selected as the most common representatives of the most common polyphenol classes in plants and in our diet, *i.e.* phenolic acids, flavanols and flavonols, respectively. GA and CA are typically involved in ester bonds with polyols (*e.g.*, quinic acid, sugars) and, in the case of GA, with flavanols (via the C3-OH group). Catechin and its epimer epicatechin are the most common units of flavanol oligomers (proanthocyanidins), a very abundant and probably underestimated class of polyphenols.[28] Rutin is much more abundant in plants and foods than its poorly water-soluble aglycone quercetin, which was investigated by our team in a previous work.[12]

Interpreting the coupling between metal - polyphenol interactions and subsequent redox processes is complicated by the huge sensitivity of metal autoxidation processes and redox potentials to pH and metal ligands including buffer components.[26] The same parameters are also expected to modulate the binding constant and stoichiometry of metal - polyphenol complexes (possibly also their geometry and spin state). For instance, in a neutral phosphate buffer, quercetin binds Fe^{II} but does not prevent the autoxidation of Fe^{II} into Fe^{III}.[12] By contrast, in a pH 5.5 acetate buffer, quercetin binds Fe^{III} and reduces it into Fe^{II}.[18] In 0.1 M HCl – MeOH (1:1),[12] quercetin does not bind Fe^{III} but still efficiently reduces it into Fe^{II} while in slightly less acidic hydroalcoholic solution (pH 2), formation of 1:1 and 2:1 Fe^{III}–quercetin complexes and subsequent electron transfers can be evidenced.[29] Finally, in neutral N-containing buffers (HEPES, MES), quercetin and phenolic acids with a catechol or pyrogallol group were shown to catalyze the autoxidation of Fe^{II} into Fe^{III} while monohydroxylated benzoic acids displayed inhibitory activities.[20,21]

In this work, a neutral moderately concentrated (10 mM) phosphate buffer was used to set the pH constant and also simply mimic the competition polyphenols may encounter in natural media with other common oxygenated ligands (organic acids, phosphate and phosphatidyl groups…) for metal ions.

3.1 Iron binding

In a neutral phosphate buffer, some common characteristics of iron – phenol binding can be outlined. Most importantly, the spectral changes following Fe^{II} addition are much faster and more intense than with Fe^{III} and a weak and broad absorption band in the range 450 – 700 nm appears that is typical of a catechol-to-Fe^{III} charge transfer band (Figs 1 & 2).[21] The latter observation

Food & Function Accepted Manuscript

suggests a fast autoxidation of Fe^{II} to Fe^{III}, which is fully confirmed by the titration of Fe^{II} through its complex with ferrozine (Fig. 3A). Thus, Fe^{II} – polyphenol binding does not provide protection to Fe^{II} against autoxidation and, based on the literature,[20,21] is even expected to accelerate the conversion of Fe^{II} into Fe^{III} due to the intrinsically higher affinity of catechols for Fe^{III}.[15] In our system, Fe^{II} autoxidation is too fast to confirm this acceleration. However, from the kinetic differences observed between Fe^{II} – polyphenol binding and Fe^{III} – polyphenol binding, it is clear that the fastest event is Fe^{II} – polyphenol binding and not autoxidation of free Fe^{II}.

In the neutral phosphate buffer, slow Fe^{III} – phenol binding can be ascribed to a competition between phosphate ions and phenols for Fe^{III}. This competition was already outlined with quercetin in our previous work by showing that Fe^{III} – quercetin binding is much faster when Fe^{III} is added last (from a concentrated solution in MeOH) than when Fe^{III} is incubated first in the phosphate buffer.[12] Overall, the most efficient route toward the Fe^{III} - catechol complex is to mix Fe^{II} and the phenol and rely on the autoxidation of the complex thus rapidly formed.

With each phenol, some specific behaviors can be singled out as described below.

Gallic acid. The kinetic analysis shows that after Fe^{II} addition, A(550 nm) rapidly increases to reach a stable plateau value A_p(550 nm) after *ca*. 2 min. The plot of $A_p - A_0$ at 550 nm *vs*. the total metal concentration can be quantitatively analyzed according to a 1:1 binding model (eqns (1) & (2), c: total phenol concentration, M_t: total metal concentration), thus yielding the corresponding apparent binding constant: K = 110 (± 32) x10^3 M^{-1} (Fig. 4, $\varepsilon_{complex}$ = 2030 (± 80) M^{-1} cm^{-1}, r = 0.998). The same analysis at 295 nm (with correction for the absorption of the free iron ion) gives fully consistent results: K = 112 (± 41) x10^3 M^{-1} ($\varepsilon_{complex}$ = 8230 (± 270) M^{-1} cm^{-1}, r = 0.999). After Fe^{III} addition, the absence of significant increase of A(550 nm) over 2 min clearly points to the very slow binding of Fe^{III} to gallic acid.

$$A = \frac{\varepsilon_{complex} K[M]c}{1 + K[M]} \quad (1)$$

$$[M] = \frac{M_t}{1 + \frac{Kc}{1 + K[M]}} \quad (2)$$

A quantitative kinetic analysis of the time dependence of A(550 nm) after Fe^{II} addition shows that the process is actually biphasic and can be interpreted by a fast bimolecular binding followed by a first-order evolution of the complex (Table 1). To take into account the overall reversibility of the process, both steps must be considered reversible. Hence, the A(550 nm) *vs*. time curves were fitted against a kinetic scheme involving the following parameters: rate constants

Food & Function Accepted Manuscript

k_1 and k_{1r} for the formation and dissociation of the first complex, respectively, rate constants k_2 and k_{2r} for the formation and dissociation of the second complex, respectively, and the molar absorption coefficients of both complexes. The additional constraints were used: the molar absorption coefficient of the second complex is set to the value previously determined at equilibrium. Rate constant k_{1r} is removed from the unknown by using: $K = k_1k_2/(k_{1r}k_{2r})$. Good curve-fittings were obtained. Rate constants k_1 and k_2 were found dependent on the total Fe^{II} concentration (Table 1), which means that our scheme is only a simplified one. A possible explanation could be that partial autoxidation of the iron – GA complexes also takes place (see H_2O_2 titration below). Anyway, the global picture emerging from this analysis is a fast and reversible Fe^{II} - GA binding with subsequent fast autoxidation of Fe^{II} into Fe^{III}, then making possible additional (reversible) phosphate coordination.

Caffeic acid. Adding iron ions to a caffeic acid solution induces a new absorption in the range 340 - 380 nm. With both iron ions, the kinetic analysis at 360 nm shows a two-step process (Fig. 2A, Table 2): the fast bimolecular formation of the metal complex (rate constant k_1), followed by an apparent first-order step (rate constant k_2) during which A(360 nm) either slowly increases (Fe^{III} case) or more rapidly decreases (Fe^{II} case) depending on the initial redox state of iron. With Fe^{II}, the same kinetic profile is observed at 600 nm (data not shown). After Fe^{II} addition, it is proposed that a Fe^{II} - CA complex is rapidly formed with subsequent fast Fe^{II} autoxidation, then converted into a second Fe^{III} - CA complex involving additional phosphate coordination. No evidence for reversibility could be observed here as the final A(360 nm) value reaches a maximum with 1 equiv. Fe^{II}. After Fe^{III} addition, a first complex is slowly formed and the second step may reflect changes in the coordination sphere (possible participation of phosphate) to yield a second Fe^{III} - CA complex. However, the absence of significant absorption in the visible range suggests that iron coordination takes place *via* the carboxyl group. Thus, addition of Fe^{II} to CA solutions could be a route to metastable Fe^{III} - catechol complexes that are not formed after Fe^{III} addition.

Catechin. The absorbance at 580 nm reaches saturation for 1 equiv. Fe^{II} in agreement with an irreversible binding. Its building-up is biphasic: a fast increase featuring Fe^{II} - catechin binding with concomitant Fe^{II} autoxidation, followed by a slower first-order decay that is independent on the metal concentration (k_{obs} = 44 (± 8) x10^{-3} s^{-1}, n = 5) and may reflect Fe^{III} - phosphate coordination.

Rutin. Besides the appearance of the weak and broad visible absorption band, the addition of iron ions brings about a bathochromic shift of the low-energy absorption band of rutin at 370 nm (Fig. 1B). As with CA, Fe^{III} - rutin binding is relatively slow and can be decomposed into two

Food & Function Accepted Manuscript

successive and quasi-irreversible steps (Figs 2B & 2C). It can be proposed that a first complex is formed (second-order rate constant k_1), which then evolves into a second more stable one (first-order rate constant k_2), possibly as a result of phosphate coordination. A quantitative analysis at 420 nm and 550 nm assuming a 1:1 stoichiometry for the complexes allows the determination of the parameters (Table 3). The k_1 and k_2 values are not significantly dependent on the total iron concentration and are reasonably consistent whether the analysis is conducted at 420 or 550 nm.

The same analysis with Fe^{II} shows that the binding is faster (Figs 2B & 2C, Table 3) as the likely consequence of a weaker competition between rutin and phosphate for Fe^{II}. A second step can also be evidenced by a weak decay of A(420 nm). Following the addition of Fe^{II}, a first complex is thus rapidly formed ($k_1 \approx 10^4$ $M^{-1}s^{-1}$) that strongly absorbs light at 420 and 550 nm in agreement with a Fe^{III} – catechol structure. However, this first complex rapidly evolves toward a second complex having spectral characteristics close to those of the final complex formed after Fe^{III} addition.

With the 4 phenols, the production of H_2O_2 over the few minutes following iron addition was generally negligible (Fig. 5) with the notable exception of gallic acid with both Fe^{II} and Fe^{III}, (20-30 % H_2O_2) and to a lesser degree caffeic acid with Fe^{II} only (*ca*. 15% H_2O_2).

3.2 Copper binding

Overall, copper – phenol binding is fast, irreversible and gives rise to much stronger spectral changes than iron – phenol binding (Fig. 6). Unlike iron titration, copper titration outlines that (with the possible exception of rutin, see below) the low-valence ion is now the stable one and that Cu^{II} is rapidly reduced (Fig. 3B) in agreement with previous observations with different phenols.[12,18,19,30] Consistently, HPLC-MS analysis permits the detection of Cu^{I} complexes of the phenols and their oxidation products (Table 4). Moreover, except with rutin, the concentration of H_2O_2 produced in equimolar solutions of phenol and copper ions is significant (20 – 30 %) over the few minutes following copper addition and independent of the ion's redox state (Fig. 5). Thus, copper – phenol binding cannot be clearly dissociated from subsequent autoxidation of the complexes. With each phenol, some specific behaviors are briefly described below.

Gallic acid. Addition of copper ions leads to a fast increase of A(330 nm) to a plateau value (Fig. 1A), followed in the case of Cu^{I} by a slight decrease. This plateau value increases with the total metal concentration and reaches a maximum with 1 equiv. copper ion (Fig. 4). This is evidence of an irreversible 1:1 binding. The binding is complete in less than 10 s with a second-order rate constant k_1 of the order of 10^4 $M^{-1}s^{-1}$.

Food & Function Accepted Manuscript

Caffeic acid. The spectral changes in the range 340 - 380 nm following the addition of copper ions to a neutral solution of caffeic acid are much more important than those observed with iron ions (Figs 6A & 6B). As with iron, the low-valence ion (Cu^{I}) induces the most important spectral modifications. Thus, a new absorption band with λ_{max} = 342 nm is observed a few seconds after Cu^{I} addition whereas only a shoulder emerges after Cu^{II} addition. After Cu^{I} addition, A(350 nm) rapidly increases, then slowly decreases (data not shown). The corresponding curves can be fitted with the same model as for GA (Table 2). After Cu^{II} addition, A(350 nm) also rapidly increases but stabilizes at a lower plateau value. The corresponding curves can be fitted assuming a simple 1:1 irreversible binding (Table 2).

Catechin. The binding of copper ions by catechin is fast (based on the spectral changes at 295 nm) and accompanied with the formation of colored products that are the hallmark of concomitant autoxidation (see below).

Rutin. Copper ions cause strong bathochromic shifts in the low-energy absorption band of rutin (Fig. 6C). With Cu^{II}, the binding is complete in less than 10 s ($k_1 \approx 2 - 4 \times 10^4$ $M^{-1}s^{-1}$). With Cu^{I}, the binding is slower ($k_1 \approx 4 - 6 \times 10^3$ $M^{-1}s^{-1}$) and rapidly followed by a second first-order step ($k_2 \approx 0.2$ - 0.3 s^{-1}) that becomes clearly apparent with Cu^{I} in excess (Table 3).

Unfortunately, the bathocuproin method was found inapplicable with rutin. Indeed, Cu^{I} titrations following the addition of Cu^{I} to a solution of rutin gave values out of the possible range of Cu^{I} concentration (> 100% Cu^{I}). Cu^{I} titrations following the addition of Cu^{II} to a solution of rutin suggested a fast reduction of Cu^{II} by rutin, which was not consistent with the much slower formation of rutin oxidation products (HPLC-MS analysis). Moreover, acidification of the samples to pH 1-2 by a small volume of 2 M aqueous HCl led to complex dissociation and the regeneration of the UV-visible spectrum of intact rutin. Such artefacts in Cu^{I} titration could be due to the formation of a ternary Cu^{I} – rutin – bathocuproin complex or to bathocuproin promoting the reduction of Cu^{II} by rutin. By analogy with quercetin[12] and the other phenols investigated in this work, it may however be suggested that Cu^{I}-rutin binding results in the persistence of Cu^{I} in solution.

3.3 Autoxidation without added metal ions

Gallic acid (GA) is relatively unstable when incubated in a pH 7.4 phosphate buffer at 37°C. The development of absorption around 330 nm was observed and ascribed to autoxidation. The

Food & Function Accepted Manuscript

corresponding apparent first-order rate constant was estimated at 187 (± 4) x10^{-6} s^{-1}, which means that the half-life of GA is *ca*. 1h in those conditions. Simultaneously, H_2O_2 was produced (*ca*. 60 μM from 100 μM GA after 4h). The HPLC-MS analysis reveals the formation of a dimer less polar than GA and with mass fragments corresponding to GA (C-O linkage, biarylether) and loss of 2 CO_2.

Caffeic acid (CA) is more stable than GA in the pH 7.4 phosphate buffer. Beside the two main absorption bands characteristic of caffeic acid at 285 and 310 nm, a shoulder at 390 nm slowly develops over 2h. From its first-order increase, an apparent rate constant of caffeic acid autoxidation can be estimated: k_{obs} = 82 (± 1) x10^{-6} s^{-1} (half-life ≈ 140 min). The HPLC-MS analysis shows the formation of a dimer in low concentration. The presence of fragments at *m*/*z* =179 and 177 (caffeic acid and its *o*-quinone) suggest that the dimer displays a labile C-O bond in agreement with a biarylether structure. Moreover, the autoxidation of caffeic acid is accompanied by H_2O_2 production (*ca*. 12 % after 1h). Based on the apparent rate constant of autoxidation, it can be estimated that one quarter of caffeic acid has been oxidized. Thus, 0.5 equiv. H_2O_2 is produced in those conditions.

Catechin also slowly undergoes 'spontaneous' autoxidation as evidenced by the quasi-linear accumulation of a broad absorption bands in the range 400 – 500 nm. Simultaneously, H_2O_2 is produced in low concentration (*ca*. 15 % after 4h). The HPLC-MS analysis allows the detection of a colorless dimer that is less polar than catechin and has mass fragments corresponding to catechin (C-O linkage, biarylether).

In the absence of added metal ion, HPLC analysis shows that rutin is stable over at least 10 h.

3.4 Metal-induced autoxidation

Gallic acid. Over 1h, the spectral changes of iron - gallic acid mixtures are very weak and are essentially manifested by a very slow increase of the absorbance in the range 280 - 320 nm (data not shown). In particular, the kinetics of Fe^{III} binding is indistinguishable from that of ligand autoxidation, which is only manifested by the steady accumulation of H_2O_2 (Fig. 5).

After the fast spectral changes dominated by the copper binding step, a steady increase of the absorbance in the range 340 – 440 nm is observed, which is ascribed to autoxidation. The autoxidation of gallic acid is much faster when initiated by Cu^{I} (in agreement with the corresponding H_2O_2 accumulation) and the corresponding apparent first-order rate constant linearly increases with the total Cu^{I} concentration (Fig. 7).

Food & Function Accepted Manuscript

Upon Cu^{II}-induced autoxidation of GA, the same dimer (biarylether) as the one obtained in the absence of added metal can be detected by HPLC-MS analysis (Table 4) as well as its Cu^{I} complex, which confirms the reduction of Cu^{II} into Cu^{I}. In addition, a trimer with water loss is also detected. This trimer probably displays a C-C (biaryl) linkage allowing dehydration and concomitant formation of a lactone ring. Finally, ultra-fast HPLC-MS analysis of Cu^{I}-induced autoxidation of GA revealed a complex mixture of decarboxylated dimers and oxidized dimers with loss or gain of H_2O molecules (Table 5).

Dioxygen titration shows that O_2 consumption following Fe^{III} or Cu^{II} addition is negligible in the absence of GA (undetectable with Fe^{III}) but becomes significant in the presence of GA, although slow and essentially independent of the metal concentration (Table 6). Dioxygen consumption from equimolar Fe^{III} - GA mixtures is consistent with H_2O_2 accumulation (Fig. 8) and shows that GA is able to reduce Fe^{III} to Fe^{II}, which does not accumulate (Fig. 3A) and is rapidly oxidized by O_2. The ability of plant phenols to reduce Fe^{III} to Fe^{II} has already been evidenced in acidic conditions.[12,18,19,29,31] Reduction was also proposed to partially occur in a neutral phosphate buffer.[17] As expected, O_2 consumption is much faster with Fe^{II} and Cu^{I} (Fig. 8). Moreover, the concentration of consumed O_2 is higher with Cu^{I} than with Fe^{II}. Both the apparent rate constants and total concentration of consumed O_2 are only marginally affected by GA.

Caffeic acid. Spectroscopic monitoring over 1h after Fe^{II} addition reveals that, after the fast binding step, A(350 nm) rapidly decays, then levels off, while it continuously increases after Fe^{III} addition (Fig. 9). The final A(350 nm) values are close with both ions. Moreover, acidification after 1h triggers the dissociation of the iron complexes and allows the recovery of the CA spectrum. However, H_2O_2 production, although modest with Fe^{II}, is significant with Fe^{III} (Fig. 5). It may thus be proposed that the spectral changes over the first 20 min that follow iron addition essentially reflect binding, Fe^{II} oxidation and possible changes in the coordination sphere of iron due to phosphate coordination but that CA autoxidation then becomes significant in Fe^{III} - CA mixtures due to the ability of CA to slowly reduce Fe^{III}.

After the fast Cu^{II} - CA binding, A(350 nm) starts to slowly decrease after a lag period of a few minutes while it more rapidly decays with the Cu^{I} - CA pair (Fig. 9). This decay is biexponential with a fast component that is essentially independent of the copper concentration: k_1 = 7.8 (± 0.9) x10^{-3} s^{-1} (n = 4) for Cu^{I} and 5.5 (± 1.8) x10^{-3} s^{-1} (n = 4) for Cu^{II}. However, whereas the slow component is independent of the Cu^{II} concentration (k_2 = 2.2 (± 0.2) x10^{-4} s^{-1}, n = 4), it linearly increases with the Cu^{I} concentration ($k_2 = 4.8M_t + 2.4x10^{-4}$ s^{-1}, r = 0.993). With the copper ions, acidification after 1h does not allow the recovery of the intact CA spectrum, thus showing that CA autoxidation has taken place. With Cu^{I}, the absence of lag phase in the decay of A(350 nm) and the more important H_2O_2 production (Fig. 5) suggest that CA autoxidation is much faster than

Food & Function Accepted Manuscript

with Cu^{II}. By comparison with GA, it can be proposed that the slow component in the decay of *A*(350 nm) is due to CA autoxidation.

HPLC-MS analysis of Cu^{II}-induced caffeic acid autoxidation confirms the formation of a dimer (already observed upon autoxidation without added metal ion) and an oxidized dimer, both of the C-O type and with concomitant decarboxylation (Table 4). Finally, ultra-fast HPLC-MS analysis of Cu^{I}-induced autoxidation of CA revealed a complex mixture of oligomers with possible additional steps of oxidation, decarboxylation and loss or gain of H_2O molecules (Table 5). Such oligomers were also evidenced when caffeic acid is oxidized by peroxyl radicals[32] or in presence of the enzyme tyrosinase.[33]

Catechin. The autoxidation rate was estimated by monitoring the color development over 1h (Fig. 10). Whatever the iron concentration and redox state, iron-induced autoxidation of catechin is very slow (indistinguishable from autoxidation without added metal). By contrast, copper-induced autoxidation (monitored at 440 or 480 nm) is very significant, especially with Cu^{I}. Despite the fast reduction of Cu^{II} to Cu^{I}, autoxidation induced by Cu^{II} is much slower (in agreement with H_2O_2 production) and largely independent of the initial Cu^{II} concentration: k_{obs} = 11.3 (± 2.1) x10^{-5} s^{-1} (n = 8). On the other hand, the rate of Cu^{I}-induced autoxidation increases with the initial Cu^{I} concentration: $k_{obs} = k_1 M_t + k_0$ with k_1 = 11.0 (± 1.2) M^{-1} s^{-1} and k_0 = 16 (± 10) x10^{-5} s^{-1}, (r = 0.96, n = 7).

The products formed during Cu^{II}–induced autoxidation of catechin (Table 4) are in agreement with those formed during the oxidation catalyzed by the copper-containing plant enzyme polyphenol oxidase:[34] a colorless dimer of the biarylether type (resulting from the electrophilic attack of the catechin semiquinone radical on the electron-rich A-ring of a second catechin molecule) already detected during spontaneous autoxidation, a colorless dimer of the biaryl type more probably resulting from a non radical coupling between the catechin *o*-quinone and the A-ring of a second catechin molecule, and two colored dimers stemming from the latter dimer by two-electron oxidation and intramolecular cyclization of the dimeric *o*-quinone thus formed. This mechanism is consistent with the observation of short induction phases prior to color development.

Rutin. Based on the stability of *A*(400 nm) and HPLC-MS analysis, autoxidation of rutin within the iron complexes seems negligible over 1h (low concentrations of oxidation products detected after 24h). By contrast, in the presence of copper ions (≥ 1 equiv.), a steady decay of *A*(400 nm) is observed, which is much more pronounced with Cu^{I} (Fig. 6C). Analysis according to an exponential model yields the apparent rate constant of Cu^{I}-induced autoxidation, which is approximately independent of the Cu^{I} concentration: k_{obs} = 35 (± 7) x10^{-5} s^{-1} (n = 5).

Food & Function Accepted Manuscript

Upon Cu^{II}-induced autoxidation, several rutin dimers were evidenced by ultra-fast HPLC-MS analysis (Fig. 11). Most were more polar than rutin (shorter retention times). All dimers display a low-energy absorption band shifted by *ca*. 10 nm to lower values with respect to rutin as well as mass fragments corresponding to the successive loss of the 2 rutinose moieties. Dimerization was also observed in the laccase-catalyzed oxidation of quercetin 3-O-β-D-glucoside.[35]

Dioxygen titration following metal addition essentially shows the same trend as with gallic acid. In particular, a weak O_2 consumption was detected in Fe^{III} – rutin mixtures (Table 6) showing that despite the low H_2O_2 production (Fig. 5) rutin undergoes a slow autoxidation in the presence of Fe^{III}.

4 Discussion

4.1 General considerations

The major points in this investigation of the reactivity of common phenols with copper and iron ions in a neutral phosphate buffer can be summarized as follows:

- Because of competing Fe^{III} - phosphate binding, the affinity of gallic acid, caffeic acid and rutin for Fe^{III} is much lower than for Fe^{II}. With caffeic acid and rutin, Fe^{II} binding is irreversible. With gallic acid, a reversible binding was observed. The binding kinetics is typically biphasic: a first complex is rapidly formed with subsequent fast Fe^{II} autoxidation. Then, a second step ascribed to additional phosphate coordination is observed.
- None of the 4 phenols protects Fe^{II} against autoxidation. During this step, ligand oxidation is marginal and H_2O_2 production, although significant with CA and GA (Fig. 5), remains lower than the 50% value predicted by overall reaction (1):

$$2\ \text{Catechol-Fe}^{II} + O_2 + 2H^+ \rightarrow 2\ \text{Catechol-Fe}^{III} + H_2O_2 \qquad (1)$$

Thus, it is proposed that a four-electron reduction of O_2 also takes place (overall reaction (2)) and that the oxidizing intermediates of this reaction do not significantly react with the phenolic ligand:

$$4\ \text{Catechol-Fe}^{II} + O_2 + 4H^+ \rightarrow 4\ \text{Catechol-Fe}^{III} + 2H_2O \qquad (2)$$

Food & Function Accepted Manuscript

Consistently, the ratio of the concentration of consumed O_2 to the initial Fe^{II} concentration is only slightly lower than the theoretical value of 0.25 deduced from reaction (2) by assuming total Fe^{II} autoxidation (Table 6).

- In agreement with the sensitivity of Fe^{II} to autoxidation, none of the 4 phenols allows Fe^{II} accumulation from Fe^{III}. However, after 1h, H_2O_2 production in equimolar solutions of Fe^{III} and GA or CA is significant (Fig. 5), respectively 55% and 38%. Thus, both gallic and caffeic acids, in weak interaction with Fe^{III}, must significantly reduce Fe^{III} into Fe^{II}, which is oxidized back to Fe^{III} as soon as formed (quasi-stationary state) with concomitant steady accumulation of H_2O_2. This is also consistent with the slow O_2 consumption observed in Fe^{III} – GA mixtures.

In the process, GA and CA are slowly oxidized to dimers according to overall reaction (3):

$$2\ \text{Catechol-Fe}^{III} + O_2 + 2H^+ \rightarrow \text{Dimer-2Fe}^{III} + H_2O_2 \qquad (3)$$

Despite the very weak H_2O_2 production (2-3 % after 1h), O_2 consumption is significant in Fe^{III} – rutin mixtures (although *ca*. twice as weak as with GA). It may thus be proposed that the rutin-Fe^{III} complex slowly evolves according to overall reaction (4):

$$4\ \text{Catechol-Fe}^{III} + O_2 + 4H^+ \rightarrow 2\ \text{Dimer-2Fe}^{III} + 2H_2O \qquad (4)$$

- The selected phenols rapidly and irreversibly bind copper ions. As expected from the total charge on the metal center, the binding is slightly faster with Cu^{II} than with Cu^{I}, thus indicating that competition between phenols and phosphate for Cu^{II} is much less important than with Fe^{III}. Except with rutin, H_2O_2 is significantly released (20-30 %) a few minutes after copper addition (Fig. 5).

- With Cu^{I}, electrons are transferred from the complex to O_2 with H_2O_2 formation and no change in the redox state of the metal center (reaction (5)):

$$2\ \text{Catechol-Cu}^{I} + O_2 + 2H^+ \rightarrow \text{Dimer-2Cu}^{I} + H_2O_2 \qquad (5)$$

After 1h, the H_2O_2 concentration with GA, CA and catechin (equimolar concentrations of phenol and Cu^{I}) is even higher than the 50% value (half the Cu^{I} concentration) predicted by reaction (5), in agreement with the detection of oxidized dimers (possible formation by reaction (6)) by ultra-fast HPLC-MS analysis:

$$\text{Dimer-2Cu}^{I} + O_2 \rightarrow \text{oxDimer-2Cu}^{I} + H_2O_2 \qquad (6)$$

Food & Function Accepted Manuscript

It is also noteworthy that the formation of *o*-quinone intermediates (consistent with the appearance of broad absorption bands in the range 350 – 450 nm, see Figs 6A & 6B in the case of caffeic acid) would allow a stoichiometric production of H_2O_2 according to reaction (7):

$$\text{Catechol-}Cu^{I} + O_2 + 2H^{+} \rightarrow o\text{-Quinone-}Cu^{I} + H_2O_2 \quad (7)$$

Quinones themselves are liable to evolve toward dimers and oxidized dimers by reacting with a phenol molecule and a second quinone molecule, respectively. Finally, the apparent rate constant of Cu^{I}-induced phenol autoxidation (k_{obs}) increases with the Cu^{I} concentration. It is thus proposed that the catechol - Cu^{I} complexes can undergo autoxidation not only by direct reaction with O_2 (within a ternary catechol - Cu^{I} - O_2 complex) but also with O_2 bound at a second metal center when Cu^{I} is in excess. For instance, reaction (8) could also contribute as already proposed in the Cu^{II}-induced autoxidation of catechol:[36]

$$\text{Catechol-}Cu^{I} + Cu^{I}\text{-}O_2 + 2H^{+} \rightarrow o\text{-Quinone-}Cu^{I} + Cu^{I} + H_2O_2 \quad (8)$$

From reactions (7) and (8), k_{obs} can be expressed as: $k_{obs} = k_7 + k_8K[Cu^{I}]$, k_7 and k_8 being the apparent first-order rate constants of reactions (7) and (8), respectively, and K the apparent thermodynamic constant of the Cu^{I}/Cu^{I}-O_2 equilibrium. On the other hand, with an excess Cu^{I}, unbound Cu^{I} must be rapidly oxidized to Cu^{II} with concomitant release of H_2O_2, which could also take part in the oxidation of the catechol - Cu^{I} complex (reaction 9):

$$\text{Catechol-}Cu^{I} + H_2O_2 + 2H^{+} \rightarrow o\text{-Quinone-}Cu^{I} + 2H_2O \quad (9)$$

The ratio of the concentration of consumed O_2 to the initial Cu^{I} concentration ($\Delta C_{O2}/M_t$) is higher than 1 when the phenol is in excess, *ca*. 1 in equimolar mixture of Cu^{I} and phenol and tends toward 0.4 – 0.5 when Cu^{I} is in excess (Table 7). The observation that the rate and extent of O_2 consumption is largely independent of the phenol being present or not is somewhat surprising as the phenols are oxidized and prevent the autoxidation of Cu^{I}. In fact, O_2 must react with Cu^{I} as rapidly as with the catechol - Cu^{I} complexes. With an excess Cu^{I}, H_2O_2 is formed by two-electron reduction of O_2 with Cu^{I} (2 equiv.) acting as the electron donor in the absence of phenol. By contrast, in the presence of a phenol, Cu^{I} simply acts as the activator permitting the transfer of 2 electrons from the catechol to O_2. This mechanism is consistent with reactions (5) and (8), which both correspond to $\Delta C_{O2}/M_t = 0.5$. It implies that Cu^{I} remains bound to the phenol's oxidation products so as to avoid its subsequent oxidation to Cu^{II}. On the other hand, with low Cu^{I} concentrations, $\Delta C_{O2}/M_t$ values higher than 0.5 rather suggest that reaction (7) prevails. In such

Food & Function Accepted Manuscript

conditions, when no phenol is present, high $\Delta C_{O2}/M_t$ values are indicative that some electron donors are still available. It may for instance be proposed that O_2 activated by Cu^I, which may be represented by Cu^{II}-$OO^{\bullet}$, can abstract one H-atom from MeOH (5% in all solutions), thereby opening additional routes for O_2 consumption (e.g., $^{\bullet}CH_2OH + O_2 \rightarrow HO\text{-}CH_2\text{-}OO^{\bullet}$).

- With Cu^{II}, ligand oxidation is slower (with a lag phase of a few minutes) in agreement with a much slower rate of O_2 consumption. The mechanism involves a rate-limiting first step of Cu^{II} reduction into Cu^I by the phenols. As the apparent rate constant of phenol autoxidation is independent on the initial Cu^{II} concentration, it may be assumed that this rate-limiting step is the slow disproportionation and/or dimerization of the rapidly formed Cu^{II} – GA complex (rather than its oxidation by a second Cu^{II} equivalent) (reactions (10) and (11)):

2 Catechol-Cu^{II} → Dimer-2Cu^I (10)

2 Catechol-Cu^{II} → *o*-Quinone-Cu^I + Catechol-Cu^I (11)

As H_2O_2 is also produced with 1 equiv. Cu^{II}, reaction (6) could also contribute in agreement with the detection of oxidized dimers in Cu^{II}–induced autoxidation.

4.2 Kinetic analysis of the copper-induced autoxidation of gallic acid

From a detailed kinetic analysis of the O_2 consumption curves, more mechanistic insight can be provided into the first steps of copper-induced autoxidation of plant phenols. This approach is described below in the case of gallic acid as an example.

Cu^I-induced autoxidation. The kinetic scheme must take into account the observation that the first-order rate constant of O_2 consumption following Cu^I addition (7 - 8x10^{-2} s^{-1}) is not affected by GA being present or not and is much larger than the apparent first-order rate of GA autoxidation (Fig. 7) assessed from the build-up of a broad absorption band around 400 nm. Hence, the formation of the ternary Cu^I - GA - O_2 complex involved in GA autoxidation is assumed to take place *via* the successive binding of O_2 and GA to Cu^I. This hypothesis is consistent with the high rate constant of Cu^I-O_2 binding[36] (k_1 = 6x10^6 $M^{-1}s^{-1}$). In addition, Cu^{II} is formed only from free Cu^I. The simplified mechanism depicted in Scheme 2 can thus be tested.

Assuming a steady-state for Cu^IO_2, eqns (3) - (9) can be derived ($r_2 = k_2/k_{-1}$, $r_3 = k_3/k_{-1}$, see Annex):

$$-\frac{d}{dt}[O_2] = k_1[Cu^I][O_2]\left(1 - \frac{1}{1 + r_2[Cu^I] + r_3[GA]}\right) \quad (3)$$

Food & Function Accepted Manuscript

$$-\frac{d}{dt}[Cu^{I}] = k_1[Cu^{I}][O_2](1-\frac{1-r_2[Cu^{I}]}{1+r_2[Cu^{I}]+r_3[GA]}) \quad (4)$$

$$\frac{d}{dt}[Cu^{II}] = \frac{2r_2k_1[Cu^{I}]^2[O_2]}{1+r_2[Cu^{I}]+r_3[GA]}) \quad (5)$$

$$-\frac{d}{dt}[GA] = \frac{r_3k_1[Cu^{I}][GA][O_2]}{1+r_2[Cu^{I}]+r_3[GA]}) \quad (6)$$

$$\frac{d}{dt}[Cu^{I}GAO_2] = \frac{r_3k_1[Cu^{I}][GA][O_2]}{1+r_2[Cu^{I}]+r_3[GA]}) - k_4[Cu^{I}GAO_2] \quad (7)$$

$$\frac{d}{dt}[H_2O_2] = \frac{r_2k_1[Cu^{I}]^2[O_2]}{1+r_2[Cu^{I}]+r_3[GA]}) + k_4[Cu^{I}GAO_2] \quad (8)$$

$$\frac{d}{dt}[Cu^{I}Q] = k_4[Cu^{I}GAO_2] \quad (9)$$

Taking k_1 = 6x10^6 M^{-1}s^{-1}, a r_2 value of 0.40 (± 0.02) M^{-1} was estimated from a curve-fitting (r = 0.99) of the control O_2 consumption experiment (no GA) with 100 µM Cu^I (due to possible contamination by undefined reducing agents, the effective Cu^I concentration was optimized at 138 (± 1) µM to take into account the overall O_2 consumption). Then, a curve-fitting (r = 0.97) of the O_2 consumption experiment with GA and Cu^I in equimolar 50 µM concentration, a r_3 value of 2.1 (± 0.2) M^{-1} was obtained, k_4 being set constant at 10^{-3} s^{-1}. The same procedure with 100 µM Cu^I (k_4 being set constant at 1.5x10^{-3} s^{-1}) gave: r_3 = 1.6 (± 0.1) M^{-1} (r = 0.99). It may thus be estimated that Cu^IO_2 reacts with GA *ca*. 4-5 times as rapidly as with Cu^I ($k_3/k_2 \approx$ 4-5). From these values, a graph representing the time dependence of GA and its complex and oxidation product can be plotted (Fig. 12A).

Cu^{II}-induced autoxidation. This phenomenon requires the preliminary reduction of Cu^{II} by GA, so as to initiate the set of reactions depicted in Scheme 2. Assuming a rate-limiting step of Cu^{II} – GA disproportionation (Scheme 3) and a steady-state for the Cu^I – GA complex thus formed, the rate of O_2 consumption can be written as: $R_{O2} = k_6[Cu^{II}\text{-GA}]^2$ (see Annex). From the initial slope of the O_2 concentration *vs*. time curve, an estimate of the disproportionation rate constant can thus be obtained: k_6 = 15 M^{-1}s^{-1}. From this model, a graph representing the time dependence of the copper complexes and the oxidation product can be plotted (Fig. 12B).

5 Conclusion

Food & Function Accepted Manuscript

This work shows that common phenols in neutral phosphate buffer rapidly bind Fe^{II}, Cu^{II} and Cu^{I} but bind Fe^{III} much more slowly because of the competing phosphate ligands. Concerning the iron complexes, despite the fast autoxidation of Fe^{II}, the phenolic ligands are only slowly oxidized and H_2O_2 production is weak, especially with the flavonoids rutin and catechin. This is consistent with the general view that iron - polyphenol binding is a potential mechanism for antioxidant protection. It must however be noted that this antioxidant mechanism with Fe^{III} is expected to be hampered when competing oxygen-containing ligands are available. It may be also less efficient with phenolic acids, which lead to higher H_2O_2 production.

Plant phenols are much more reactive with O_2 when bound to copper than to iron. Our results suggest that electrons are readily transferred from the phenolic ligands to O_2 within the ternary Phenol - Cu^{I} - O_2 complexes without change in the redox state of copper. By contrast, in the corresponding Phenol - Fe^{II} - O_2 complexes, electrons are transferred from Fe^{II} with concomitant formation of the Fe^{III} - Phenol complexes. These reactions can also take place from the Fe^{III} - Phenol and Cu^{II} - Phenol complexes but are hampered by the preliminary slow step of Fe^{III} and Cu^{II} reduction by the phenols. These points are summarized on Scheme 4.

Overall, copper ions come up as much more critical to plant phenol stability than iron ions. The following ranking in sensitivity to copper-induced autoxidation can be proposed: gallic acid > caffeic acid ≈ catechin > rutin. Copper-induced autoxidation of plant phenols and concomitant H_2O_2 production is expected to limit the antioxidant activity of plant phenols when copper ions are used to initiate oxidative stress. It must however be kept in mind that this chemistry rests on the ability of plant phenols to bind metal ions, a property strongly dependent on pH and other competing ligands. For instance, the selected phenols do not bind copper ions in a 0.1 M acetate buffer at pH 5 (data not shown). On the other hand, the pH of the upper gastro-intestinal tract may vary from pH 2 (empty stomach) to mildly acidic / neutral conditions (stomach after meal consumption, small intestine).[37] Hence, it is important to go beyond simple models (amenable to mechanistic investigations) and also develop more realistic models to further test the relevance of metal – phenol chemistry in food and in the digestive tract.

6 Annex: kinetic analysis of copper-induced phenol autoxidation

6.1 Autoxidation induced by Cu^{I}

Based on Scheme 2, the following rate laws can be derived:

Food & Function Accepted Manuscript

$$-\frac{d}{dt}[O_2] = k_1[Cu^I][O_2] - k_{-1}[Cu^IO_2] \quad (1)$$

$$-\frac{d}{dt}[Cu^I] = k_1[Cu^I][O_2] - k_{-1}[Cu^IO_2] + k_2[Cu^I][Cu^IO_2] \quad (2)$$

$$-\frac{d}{dt}[Cu^{II}] = 2k_2[Cu^I][Cu^IO_2] \quad (3)$$

$$-\frac{d}{dt}[GA] = k_3[Cu^IO_2][GA] \quad (4)$$

$$\frac{d}{dt}[Cu^IGAO_2] = k_3[Cu^IO_2][GA] - k_4[Cu^IGAO_2] \quad (5)$$

$$\frac{d}{dt}[H_2O_2] = k_2[Cu^I][Cu^IO_2] + k_4[Cu^IGAO_2] \quad (6)$$

$$\frac{d}{dt}[Cu^IQ] = k_4[Cu^IGAO_2] \quad (7)$$

Assuming a steady-state for Cu^IO_2, one has:

$$k_1[Cu^I][O_2] = [Cu^IO_2](k_{-1} + k_2[Cu^I] + k_3[GA])$$

Or

$$\frac{k_1}{k_{-1}}[Cu^I][O_2] = [Cu^IO_2](1 + r_2[Cu^I] + r_3[GA]) \quad (8)$$

With $r_2 = k_2/k_{-1}$, $r_3 = k_3/k_{-1}$.

Replacing $[Cu^IO_2]$ in eqns (1)-(6) by its expression deduced form eqn (8) readily gives eqns (3) - (9) (see text).

6.2 Autoxidation induced by Cu^{II}

Based on Schemes 2 & 3, the following rate laws can be derived:

$$-\frac{d}{dt}[O_2] = k_{1b}[Cu^IGA][O_2] - k_{-1b}[Cu^IGAO_2] \quad (1)$$

$$-\frac{d}{dt}[Cu^{II}] = -\frac{d}{dt}[GA] = k_5[Cu^{II}][GA] \quad (2)$$

$$\frac{d}{dt}[Cu^{II}GA] = k_5[Cu^{II}][GA] - 2k_6[Cu^{II}GA]^2 \quad (3)$$

$$\frac{d}{dt}[Cu^IGA] = k_6[Cu^{II}GA]^2 - k_{1b}[Cu^IGA][O_2] + k_{-1b}[Cu^IGAO_2] \quad (4)$$

Food & Function Accepted Manuscript

$$\frac{d}{dt}[Cu^{I}GAO_2] = k_{1b}[Cu^{I}GA][O_2] - k_{-1b}[Cu^{I}GAO_2] - k_4[Cu^{I}GAO_2] \quad (5)$$

$$\frac{d}{dt}[H_2O_2] = k_4[Cu^{I}GAO_2] \quad (6)$$

$$\frac{d}{dt}[Cu^{I}Q] = k_4[Cu^{I}GAO_2] + k_6[Cu^{II}GA]^2 \quad (7)$$

Assuming a steady-state for $Cu^{I}GA$, one has:

$$k_{1b}[Cu^{I}GA][O_2] = k_{-1b}[Cu^{I}GAO_2] + k_6[Cu^{II}GA]^2$$

$$-\frac{d}{dt}[O_2] = k_6[Cu^{II}GA]^2 \quad (1)$$

$$-\frac{d}{dt}[Cu^{II}] = -\frac{d}{dt}[GA] = k_5[Cu^{II}][GA] \quad (2)$$

$$\frac{d}{dt}[Cu^{II}GA] = k_5[Cu^{II}][GA] - 2k_6[Cu^{II}GA]^2 \quad (3)$$

$$\frac{d}{dt}[Cu^{I}GAO_2] = k_6[Cu^{II}GA]^2 - k_4[Cu^{I}GAO_2] \quad (4)$$

$$\frac{d}{dt}[H_2O_2] = k_4[Cu^{I}GAO_2] \quad (5)$$

$$\frac{d}{dt}[Cu^{I}Q] = k_4[Cu^{I}GAO_2] + k_6[Cu^{II}GA]^2 \quad (6)$$

Food & Function Accepted Manuscript

References

1 S. Quideau, D. Deffieux, C. Douat-Casassus and L. Pouysegu, Plant polyphenols: chemical properties, biological activities, and synthesis, *Angew. Chem. Int. Ed*., 2011, **50**, 586-621.

2 V. Neveu, J. Perez-Jimenez, F. Vos, V. Crespy, L. du Chaffaut, L. Mennen, C. Knox, R. Eisner, J. Cruz, D. Wishart and A. Scalbert, 2010, Phenol-Explorer: an online comprehensive database on polyphenol contents in foods, http://www.phenol-explorer.eu.

3 J. Perez-Jimenez, L. Fezeu, M. Touvier, N. Arnault, C. Manach, S. Hercberg, P. Galan and A. Scalbert, Dietary intake of 337 polyphenols in French adults, *Am. J. Clin. Nutr.*, 2011, **93**, 1220-1228.

4 H. P. V. Rupasinghe, N. Erkan and A. Yasmin, Antioxidant protection of eicosapentaenoic acid and fish oil oxidation by polyphenolic-enriched apple skin extract, *J. Agric. Food Chem*., 2010, **58**, 1233-1239.

5 M.T. Escribano-Bailon and C. Santos-Buelga, Anthocyanin copigmentation - evaluation, mechanisms and implications for the colour of red wines, *Curr. Org. Chem.*, 2012, **16**, 715-723.

6 V. de Freitas and N. Mateus, *Curr. Org. Chem.*, Protein / polyphenol interactions: past and present contributions. Mechanisms of astringency perception, 2012, **16**, 724-746.

7 A. Crozier, I. B. Jaganath and M. N. Clifford, Dietary phenolics: chemistry, bioavailability and effects on health, *Nat. Prod. Rep*., 2009, **26**, 1001-1043.

8 G. Williamson and C. Manach, Bioavailability and bioefficacy of polyphenols in humans. II. Review of 93 intervention studies, *Am. J. Clin. Nutr.*, 2005, **81**, 243S-255S.

9 O. Dangles, Antioxidant activity of plant phenols: chemical mechanisms and biological significance, *Curr. Org. Chem.* 2012, **16**, 692-714.

10 F. Virgili and M. Marino, Regulation of cellular signals from nutritional molecules: a specific role for phytochemicals, beyond antioxidant activity, *Free Radical Biol. Med.*, 2008, **45**, 1205-1216.

11 S. Tokalioglu and F. Gurbuz, Selective determination of copper and iron in various food samples by the solid phase extraction, *Food Chem.*, 2010, **123**, 183-187.

12 H. El Hajji, E. Nkhili, V. Tomao and O. Dangles, Interactions of quercetin with iron and copper ions: Complexation and autoxidation, *Free Radical Res.*, 2006, **40**, 303-320.

13 C. Sy, O. Dangles, P. Borel and C. Caris-Veyrat, Iron-induced oxidation of (all-E)-β-carotene in model gastric conditions: kinetics, products and mechanism, *Free Radical Biol. Med.*, 2013, **63**, 195-206.

14 Z. Cheng and Y. Li, What is responsible for the initiating chemistry of iron-mediated lipid peroxidation: an update, *Chem. Rev*., 2007, **107**, 748-766.

Food & Function Accepted Manuscript

15 N. R. Perron and J. L. Brumaghim, A review of the antioxidant mechanisms of polyphenol compounds related to iron binding, *Cell. Biochem. Biophys*., 2009, **53**, 75-100.

16 M. D. Engelmann, R. Hutcheson and I. F. Cheng, Stability of ferric complexes with 3-hydroxyflavone (flavonol), 5,7-dihydroxyflavone (chrysin), and 3',4'-dihydroxyflavone, *J. Agric. Food Chem.*, 2005, **53**, 2953-2960.

17 M. Guo , C. Perez , Y. Wei , E. Rapoza , G. Su , F. Bou-Abdallah and N. D. Chasteen, Iron-binding properties of plant phenolics and cranberry's bio-effects, *Dalton Trans*., 2007, 4951-4961.

18 L. Mira, M. T. Fernandez, M. Santos, R. Rocha, M. H. Florencio and K. R. Jennings, Interactions of flavonoids with iron and copper ions: A mechanism for their antioxidant activity, *Free Radical Res*., 2002, **36**, 1199-1208.

19 M. T. Fernandez, M. L. Mira, M. H. Florencio and K. R. Jennings, Iron and copper chelation by flavonoids: an electrospray mass spectrometry study, *J. Inorg. Biochem*., 2002, **92**, 105-111.

20 K. Chvatalova, I. Slaninova, L. Brezinova and J. Slanina, Influence of dietary phenolic acids on redox status of iron: Ferrous iron autoxidation and ferric iron reduction, *Food Chem*., 2008, **106**, 650-660.

21 N. R. Perron, H. C. Wang, S. N. DeGuire, M. Jenkins, M. Lawson and J. L. Brumaghim, Kinetics of iron oxidation upon polyphenol binding, *Dalton Trans.*, 2010, **39**, 9982-9987.

22 J. F. Moran, R. V. Klucas, R. J. Grayer, J. Abian and M. Becana, Complexes of iron with phenolic compounds from soybean nodules and other legume tissues: prooxidant and antioxidant properties, *Free Radical Biol. Med*., 1997, **22**, 861-870.

23 M. Sakano, M. Mizutani, M. Murata, S. Oikawa, Y. Hiraku and S. Kawanishi, Procyanidin B2 has anti- and pro-oxidant effects on metal-mediated DNA damage, *Free Radical Biol. Med*., 2005, **39**, 1041-1049.

24 N. R. Perron, C. R. Garcia, J. R. Pinzon, M. N. Chaur and J. L. Brumaghim, Antioxidant and prooxidant effects of polyphenol compounds on copper-mediated DNA damage, *J. Inorg. Biochem*., 2011, **105**, 745-753.

25 E. Sodergren, J. Nourooz-Zadeh, L. Berglund and B. Vessby, Re-evaluation of the ferrous oxidation in xylenol orange assay for the measurement of plasma lipid hydroperoxides, *J Biochem. Biophys. Methods*, 1998, **37**, 137-146.

26 K. D. Welch, T. Z. Davis and S. D. Aust, Iron autoxidation and free radical generation: effects of buffers, ligands, and chelators, *Arch. Biochem. Biophys*., 2002, **397**, 360-369.

27 K. Midorikawa, T. Uchida, Y. Okamoto, C. Toda, Y. Sakai, K. Ueda, Y. Hiraku, M. Murata, S. Kawanishi and N. Kojima, Metabolic activation of carcinogenic ethylbenzene leads to oxidative DNA damage, *Chem. Biol. Int*., 2004, **150**, 271-281.

Food & Function Accepted Manuscript

28 I. Tarascou, J. M. Souquet, J. P. Mazauric, S. Carrillo, S. Coq, F. Canon, H. Fulcrand and V. Cheynier, The hidden face of food phenolic composition, *Arch. Biochem. Biophys*., 2010, **501**, 16-22.

29 P. Ryan and M. J. Hynes, The kinetics and mechanisms of the reaction of iron(III) with quercetin, *J. Inorg. Chem*., 2008, **102**, 127-136.

30 H. S. Mahal, S. Kapoor, A. K. Satpati and T. Mukherjee, Radical scavenging and catalytic activity of metal-phenolic complexes, *J. Phys. Chem. B.*, 2005, **109**, 24197-24202.

31 M. J. Hynes and M. O'Coinceanainn, The kinetics and mechanisms of reactions of iron(III) with caffeic acid, chlorogenic acid, sinapic acid, ferulic acid and naringin, *J. Inorg. Biochem*., 2004, **98**, 1457-1464.

32 M. Roche, C. Dufour, N. Mora and O. Dangles, Antioxidant activity of olive phenols: mechanistic investigation and characterization of oxidation products by mass spectrometry, *Org. Biomol. Chem*., 2005, **3**, 423-430.

33 S. Pati, I. Losito, F. Palmisano and P.G. Zambonin, Characterization of caffeic acid enzymatic oxidation by-products by liquid chromatography coupled to electrospray ionization tandem mass spectrometry, *J. Chromatogr. A*, 2006, **1102**, 184-192.

34 S. Guyot, J. Vercauteren and V. Cheynier, Structural determination of colorless and yellow dimers resulting from (+)-catechin coupling catalysed by grape polyphenoloxidase, *Phytochemistry*, 1996, **42**, 1279-1288.

35 S. Ghidouche, N.-E. Es-Safi and P.-H. Ducrot, Mechanistic study on the enzymatic oxidation of flavonols, *Tetrahedron Lett*., 2008, **49**, 619-623.

36 P. Kamau and R. B. Jordan, Kinetic study of the oxidation of catechol by aqueous copper(II), *Inorg. Chem*., 2002, **41**, 3076-3083.

37 V. Tyssandier, E. Reboul, J.-F. Dumas, C. Bougteloup-Demange, M. Armand, J. Marcand, M. Sallas and P. Borel, Processing of vegetable-borne carotenoids in the human stomach and duodenum, *Am. J. Physiol*., 2003, **284**, G913–G923.

Food & Function Accepted Manuscript

Table 1 Fe^{II} - gallic acid binding (pH 7.4 phosphate buffer, 37°C). Spectroscopic monitoring at 550 nm over 2 min. GA concentration = 50 μM.

ρ [a]	$10^{-3}k_1$ ($M^{-1}s^{-1}$)	$10^{3}k_2$ (s^{-1})	$10^{3}k_{2r}$ (s^{-1})	ε_1 ($M^{-1}cm^{-1}$)
0.5	9.5 (± 0.1)	27.4 (± 1.6)	18.2 (± 0.9)	2140 (± 20)
1	7.7 (± 0.2)	10.5 (± 2.1)	21.8 (± 3.1)	1610 (± 10)
1.5	5.0 (± 0.1)	27.7 (± 0.8)	27.4 (± 0.4)	1730 (± 10)
2	3.7 (± 0.1)	48.8 (± 1.1)	29.0 (± 0.3)	1920 (± 10)

[a] Metal ion / phenol molar ratio

Food & Function Accepted Manuscript

Table 2 Metal - caffeic acid binding (pH 7.4 phosphate buffer, 37°C). Spectroscopic monitoring at 360 nm over 2 min (Fe) or at 350 nm over 1 min (Cu). Caffeic acid concentration = 50 μM.

ρ [a]	$10^{-3}k_1$ ($M^{-1}s^{-1}$)	$10^{3}k_2$ (s^{-1})	ε_1 ($M^{-1}cm^{-1}$)	ε_2 ($M^{-1}cm^{-1}$)
Fe^{III}				
1	2.8 (± 0.3)	12 (± 1)	2560 (± 20)	3340 (± 20)
1.5	1.0 (± 0.1)	15 (± 2)	3360 (± 40)	3840 (± 20)
2	0.7 (± 0.1)	7 (± 2)	3510 (± 20)	4270 (± 110)
2.5	1.5 (± 0.1)	20 (± 2)	4000 (± 10)	4250 (± 10)
3	1.3 (± 0.1)	25 (± 6)	4210 (± 20)	4340 (± 10)
Fe^{II}				
1	9.2 (± 0.6)	81 (± 4)	11.1 (± 0.3)x10^3	5660 (± 40)
1.5	4.0 (± 0.3)	95 (± 6)	10.5 (± 0.4)x10^3	5310 (± 30)
2	4.8 (± 0.1)	65 (± 1)	8560 (± 50)	5300 (± 20)
2.5	4.4 (± 0.2)	40 (± 1)	8090 (± 60)	5580 (± 40)
Cu^{II}				
0.5	10.9 (± 0.6)	-	11.8 (± 0.1)x10^3	-
1	20.3 (± 2.4)	-	8770 (± 60)	-
1.5	20.6 (± 0.7)	-	9840 (± 20)	-
2	12.0 (± 0.3)	-	10.6 (± 0.1)x10^3	-
Cu^{I}				
0.5	2.9 (± 1.1)	281 (± 34)	56 (± 19)x10^3	18.0 (± 0.2)x10^3
1	4.4 (± 0.2)	84 (± 6)	21x10^3 [b]	12.0 (± 0.1)x10^3
1.5	4.0 (± 0.4)	153 (± 9)	21 (± 1)x10^3	11.7 (± 0.1)x10^3
2	2.1 (± 0.1)	152 (± 8)	21x10^3 [b]	11.4 (± 0.1) x10^3

[a] Metal ion / phenol molar ratio. [b] Set constant.

Food & Function Accepted Manuscript

Table 3 Metal - rutin binding (rutin conc. = 50 μM). Unless otherwise specified, spectroscopic monitoring as follows: 420 nm, 5 min (Fe^{III}), 420 nm, 1 – 2 min (Fe^{II}), 400 nm, 1 min (Cu).

ρ [a]	$10^{-3}k_1$ ($M^{-1}s^{-1}$)	$10^{3}k_2$ (s^{-1})	ε_1 ($M^{-1}cm^{-1}$)	ε_2 ($M^{-1}cm^{-1}$)
Fe^{III}				
0.5	4.0 (± 0.2)	6.1 (± 0.2)	6590 (± 30)	8990 (± 40)
0.5 [b]	4.9 (± 0.6)	5.9 (± 0.6)	680 (± 20)	1440 (± 30)
1	2.1 (± 0.1)	3.9 (± 0.4)	6220 (± 30)	7560 (± 90)
1 [b]	1.1 (± 0.2)	3.4 (± 2.0)	510 (± 50)	940 (± 150)
1.5	3.0 (± 0.1)	7.8 (± 0.3)	7620 (± 20)	8950 (± 20)
1.5 [b]	3.6 (± 0.2)	6.2 (± 0.6)	950 (± 10)	1490 (± 20)
2	2.0 (± 0.1)	10.4 (± 0.4)	7480 (± 20)	8660 (± 10)
2 [b]	1.8 (± 0.1)	8.1 (± 0.4)	950 (± 10)	1410 (± 10)
2.5	1.6 (± 0.1)	11.7 (± 0.5)	7850 (± 20)	8730 (± 10)
2.5 [b]	1.6 (± 0.1)	8.6 (± 0.4)	1120 (± 10)	1480 (± 10)
3	1.6 (± 0.1)	11.3 (± 0.5)	8300 (± 10)	8950 (± 10)
3 [b]	2.0 (± 0.1)	5.7 (± 0.9)	1290 (± 10)	1620 (± 20)
Fe^{II}				
0.5	9.1 (± 0.9)	-	16390 (± 220)	-
1	6.9 (± 1.1)	186 (± 20)	15650 (± 1160)	9890 (± 70)
1 [b]	12.2 (± 0.8)	128 (± 9)	3110 (± 100)	2100 (± 10)
1.5	11.0 (± 0.6)	253 (± 11)	11350 (± 210)	9340 (± 10)
2	13.3 (± 0.4)	195 (± 9)	10410 (± 70)	9190 (± 10)
2.5	8.6 (± 0.2)	133 (± 6)	9970 (± 40)	8770 (± 10)
Cu^{II}				
0.5	17.2 (± 0.7)	-	17140 (± 30)	-
1	43.5 (± 1.7)	-	16790 (± 20)	-
1.5	28.4 (± 1.5)	-	16770 (± 20)	-
Cu^{I}				
0.5 [c]	4.2 (± 0.5)	329 (± 13)	49500 (± 4400)	25110 (± 40)
1 [c]	6.5 (± 0.9)	160 (± 15)	26300 (± 1400)	19100 (± 80)
2	3.6 (± 0.5)	270 (± 23)	25600 (± 1800)	18620 (± 10)

[a] Metal ion/ phenol molar ratio. [b] Monitoring at 550 nm. [c] No apparent decay.

Food & Function Accepted Manuscript

Table 4 HPLC-MS analysis of the oxidation products formed during Cu^{II}-induced autoxidation (2 equiv. Cu^{II}, 7h, pH 7.4 phosphate buffer, 37°C).

t_R (min)	*m/z*	λ_{max} (nm)	Proposed structure [a]
		Gallic acid (GA)	
4.8	169, 231	228, 272	GA-H^+, GA-$2H^+$+Cu^I
10.4	487, 549	250, 296	T-H_2O-H^+, T-H_2O-$2H^+$+Cu^I
12.8 [b]	337, 399	247, 291	D-H^+, D-$2H^+$+Cu^I
		Caffeic acid (CA)	
15.7	179, 241	326, 252	CA-H^+, CA-$2H^+$+Cu^I
16.9	311, 373	337	D-2H-CO_2-H^+, D-2H-CO_2-$2H^+$+Cu^I
17.9 [b]	313	316, 260	D-CO_2-H^+
		Catechin (Cat)	
12.2	577, 639	280	D-H^+, D-$2H^+$+Cu^I
12.4	289, 351	280	Cat-H^+, Cat-$2H^+$+Cu^I
14.0 [b]	577, 639	280	D-H^+, D-$2H^+$+Cu^I
14.7	575, 637	278, 416	D-2H-H^+, D-2H-$2H^+$+Cu^I
16.2	575, 637	256, 280, 385	D-2H-H^+, D-2H-$2H^+$+Cu^I

[a] D, T = covalent dimer and trimer = (phenol-H)$_n$ (n = 2,3). Copper is a combination of two stable isotopes ^{63}Cu (69.2%) + ^{65}Cu (30.8%). The mass signal for the complex of the major isotope is reported. [b] Also observed in autoxidation without added metal.

Food & Function Accepted Manuscript

Table 5 Ultra fast HPLC-MS analysis of the oxidation products formed during Cu^{I}-induced autoxidation (2 equiv. Cu^{I}, pH 7.4 phosphate buffer, 37°C).

t_R / min	*m/z*, MS	*m/z*, MS^n	Proposed structure [a]
		Gallic acid, t = 2h	
0.8 - 1.0	445, 389, 291	445 → 427 → 383 → 355, 327 291 → 245 → 219 → 191	D + GA - CO_2 - H_2O
6.90	401, 357, 313	401 → 357 → 313 → 285	D + GA - $2CO_2$ - H_2O
7.15	291	291 → 273 → 245 → 217	D - CO_2 - 2H
8.15	263	263 → 219, 191 → 153	D - 4H - $2CO_2$ + H_2O
		Caffeic acid, t = 3h	
1.25	537	537 → 521 → 477, 459 477 → 459, 415 459 → 431, 403, 311	D + CA
2.35	375, 137	375 → 287 → 137	D + H_2O
4.50	313, 269	313 → 269 → 251 → 223	D - CO_2 (biaryl)
5.30	311	311 → 267 → 239, 197	D - CO_2 - 2H
5.50	307, 261, 187	307 → 279 → 235	D - CO_2 - 6H
5.77	313, 187	313 → 269, 179, 135 269 → 135	D - CO_2 (biarylether)
6.50	489, 445, 395, 313	445 → 309 → 281, 265 281 → 237	T - CO_2 - 2H
7.0	617, 593, 389, 321, 201	593 → 285 → 255, 217 389 → 331, 269, 203	Te - $3CO_2$ + $2H_2O$ - 2H

[a] D, T, Te = covalent dimer, trimer and tetramer = $(phenol\text{-}H)_n$ (n = 2-4), $-H^+$ omitted for all structures

Food & Function Accepted Manuscript

Table 6 Dioxygen consumption following metal addition (1 equiv., pH 7.4 phosphate buffer, 37°C). Phenol concentration = 50 μM.

[a]	k_{obs} (s^{-1})	ΔC_{max} (μM)	Δt (s)
Cu^{I}	75 (± 1) x10^{-3}	51.7 (± 0.1)	200
Cu^{I} + rutin	79 (± 2) x10^{-3}	52.1 (± 0.1)	200
Cu^{I} + GA	69 (± 2) x10^{-3}	51.6 (± 0.1)	200
Cu^{II} [b]	4 x10^{-5}	8	780
Cu^{II} + rutin	236 (± 2) x10^{-5}	30.3 (± 0.2)	780
Cu^{II} + GA	128 (± 3) x10^{-5}	34.1 (± 0.4)	1050
Fe^{II}	37 (± 2) x10^{-3}	11.3 (± 0.2)	100
Fe^{II} + GA	30 (± 1) x10^{-3}	5.2 (± 0.1) [c]	200
Fe^{II} + rutin	44 (± 2) x10^{-3}	9.5 (± 0.1)	150
Fe^{III}	nd	nd	
Fe^{III} + rutin	296 (± 5) x10^{-5}	13.8 (± 0.1)	880
Fe^{III} + GA	146 (± 3) x10^{-5}	26.6 (± 0.4)	820

[a] Curve-fitting using $\Delta C = \Delta C_{max}(1-\exp(-k_{obs}t))$ over period Δt. [b] Linear fitting, k_{obs} estimated from $R_{obs} \approx k_{obs}C_0$. [c] *ca*. 12 μM after 15 min. nd: not detectable.

Food & Function Accepted Manuscript

Table 7 Ratio of the maximal concentration of consumed O_2 to the total metal concentration following Cu^I addition (pH 7.4 phosphate buffer, 37°C, t = 1 - 3 min). Phenol concentration = 50 μM.

	$\Delta C_{max} / M_t$		
M_t / μM	control	rutin	gallic acid
25	1.80	1.61	1.87
50	1.07	1.09	1.07
100	0.61	0.69	0.77
150	0.51	0.55	0.55
200	0.44	0.51	0.50
250	0.36	0.47	0.44

Food & Function Accepted Manuscript

Legends of Figures

Fig. 1 UV-visible spectra of metal – phenol complexes (phenol and metal concentrations = 50 µM, pH 7.4 phosphate buffer, 37°C). **A:** gallic acid (spectra recorded *ca*. 2 min after mixing). 1: GA, 2: GA + Fe^{III} 3: GA + Fe^{II}, 4: GA + Cu^{II}, 5: GA + Cu^{I}. **B:** rutin (spectra recorded *ca*. 40 s after metal addition). 1: rutin, 2: Fe^{III} + rutin, 3: Fe^{II} + rutin.

Fig. 2 Kinetic monitoring of iron - phenol binding (phenol concentration = 50 µM, pH 7.4 phosphate buffer, 37°C). **A:** caffeic acid. ■: 1 equiv. Fe^{II}, ▲: 2.5 equiv. Fe^{III}, ●: 1 equiv. Fe^{III}. **B & C:** rutin. ■: 1 equiv. Fe, ●: 2 equiv. Fe.

Fig. 3 Changes in the redox state of metal ions in the presence of GA (1 equiv.). **A:** ♦ Fe^{II}, ■ GA-Fe^{III}, ▲ GA-Fe^{II}. **B:** ♦ Cu^{I}, ■ GA-Cu^{II}, ▲ GA-Cu^{I} (pH 7.4 phosphate buffer, 37°C).

Fig. 4 Plot of ΔA (absorbance amplitude of the binding step) as a function of the metal/GA molar ratio. ■: Cu^{I} (λ = 300 nm, irreversible binding, $\varepsilon_{complex}$ = 12400 $M^{-1}cm^{-1}$), ●: Fe^{II} (λ = 550 nm, K = 110 (± 32) x10^3 M^{-1}, $\varepsilon_{complex}$ = 2030 (± 80) M^{-1} cm^{-1}, r = 0.998).

Fig. 5 H_2O_2 production during autoxidation of the selected phenols (initial concentration = 100 µM) in the presence of iron and copper ions (1 equiv.). **A:** gallic acid, **B:** caffeic acid, **C:** catechin, **D:** rutin, ♦ Fe^{III}, ■ Fe^{II}, ▲ Cu^{II}, • Cu^{I} (pH 7.4 phosphate buffer, 37°C).

Fig. 6 Copper – phenol binding (phenol and Cu concentrations = 50 µM, pH 7.4 phosphate buffer, 37°C). 1: phenol (t = 0), 2: t = 2 min, 3: t = 60 min after Cu addition. **A:** CA + Cu^{I}. **B:** CA + Cu^{II}. **C:** rutin + Cu^{I}.

Fig. 7 Plot of the apparent rate constant of GA autoxidation (monitoring at 400 nm over 1h) as a function of the total copper concentration (GA concentration = 50 µM, pH 7.4 phosphate buffer, 37°C). ■: Cu^{I}, $k_{obs} = k_1 M_t + k_0$ with k_1 = 12.7 (± 0.7) M^{-1} s^{-1}, k_0 = 23 (± 7) x10^{-5} s^{-1}, r = 0.996. ●: Cu^{II}, k_{obs} = 21 (± 4) x10^{-5} s^{-1} (n = 6).

Fig. 8 Dioxygen consumption following copper addition (1 equiv., pH 7.4 phosphate buffer, 37°C). GA concentration = 50 µM. ■: Cu + GA, ●: Cu alone.

Fig. 9 Spectral changes observed after mixing caffeic acid and metal ions (CA concentration = 50 µM, metal concentration = 75 µM). Copper ions: detection at 350 nm, iron ions: detection at 360

Food & Function Accepted Manuscript

nm. After the fast increase mainly ascribed to metal binding (*ca*. 0.5 – 1 min), the biexponential fitting of the curves gives $10^4 k_1$ and $10^4 k_2$ (s^{-1}) = 92 (± 5) and 7.0 (± 1.5) (Fe^{III}), 240 (± 10) and 40 (± 1) (Fe^{II}), 86 (± 1) and 6.1 (± 0.1) (Cu^{I}) and, after a lag phase of *ca*. 4 min, 39 (± 1) and 2.1 (± 0.1) (Cu^{II}).

Fig. 10 Autoxidation of catechin (50 µM) in the presence of metal ion (1 equiv.). Spectra recorded 1 h after mixing (pH 7.4 phosphate buffer, 37°C): 1: catechin, 2 - 4: catechin + metal ion (2: Fe^{II}, 3: Cu^{II}, 4: Cu^{I}).

Fig. 11 Ultrafast HPLC-MS analysis of rutin oxidation products (2 equiv. Cu^{II}, 3h30).
A: chromatogram with UV detection at 280 nm. Peaks at t_R = 4.45, 4.55, 4.75, 4.85, 4.95, 5.10, 5.90 and 6.20 min and λ_{max} = 350 and 260 nm were all attributed to covalent dimers with typical *m*/*z* values = 1217 ((rutin-H)$_2$-H^+), 909 (idem - 1 rutinose unit), 601 (idem - 2 rutinose units), 609 (rutin-H^+). **B:** UV-visible and mass spectra of peak at t_R = 4.55 min. **C:** MS^4 analysis of peak at t_R = 4.55 min.

Fig. 12 Copper - gallic acid binding and autoxidation (pH 7.4 phosphate buffer, 37°C). Copper concentration = 100 µM. **A**: Cu^{I}, **B**: Cu^{II}.

Food & Function Accepted Manuscript

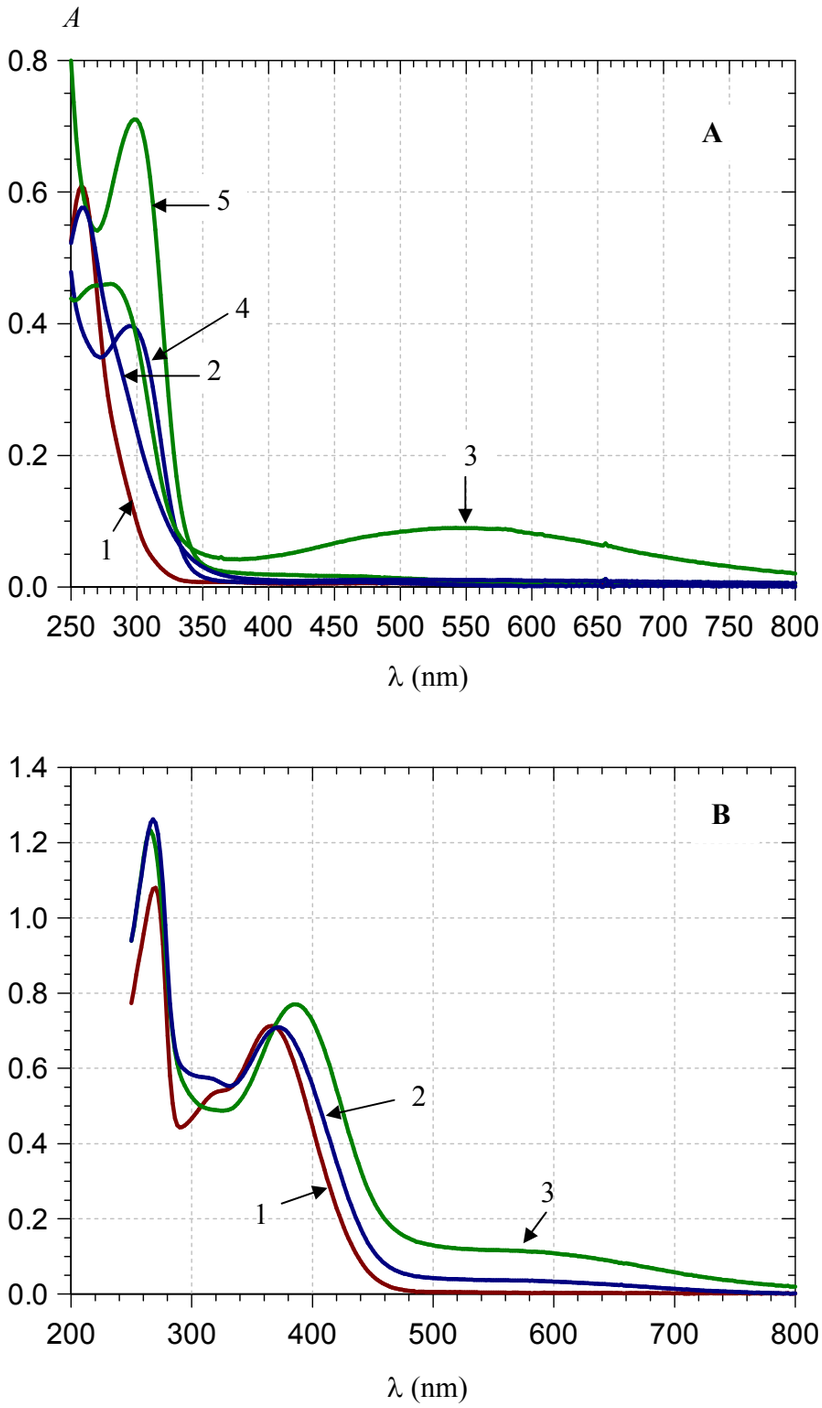

Fig. 1

Food & Function Accepted Manuscript

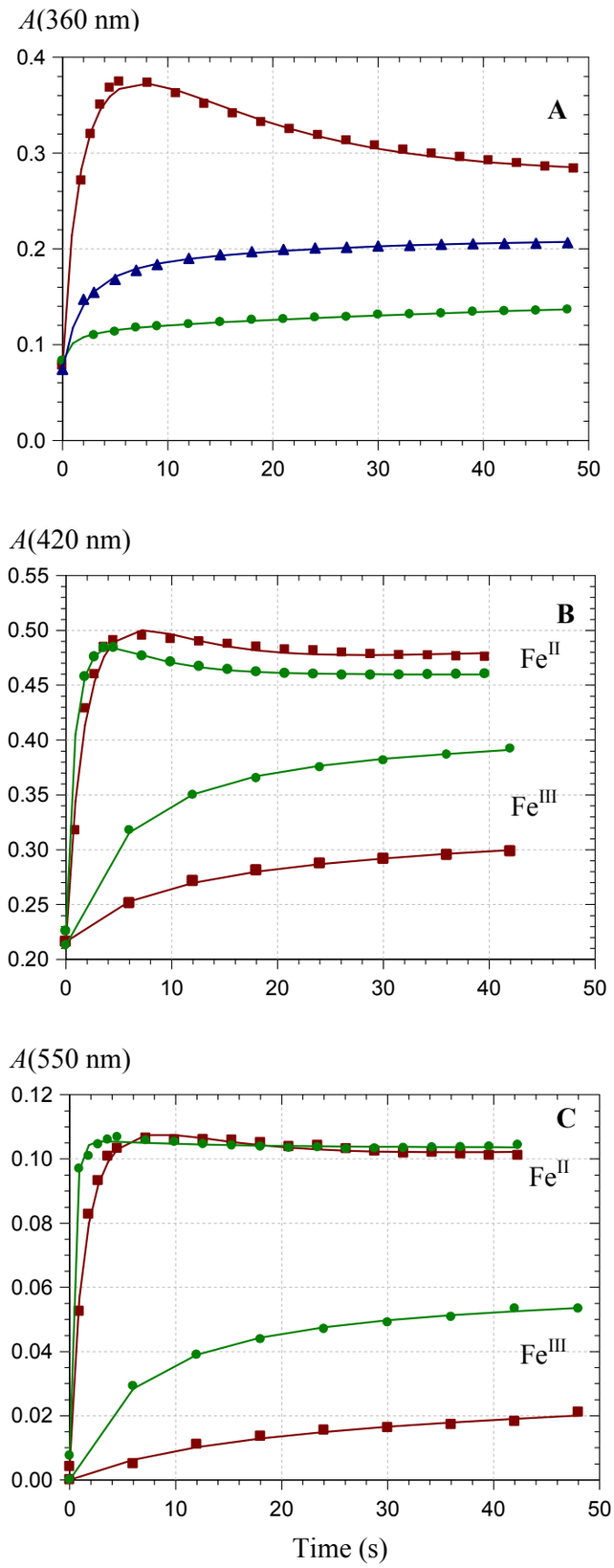

Fig. 2

Food & Function Accepted Manuscript

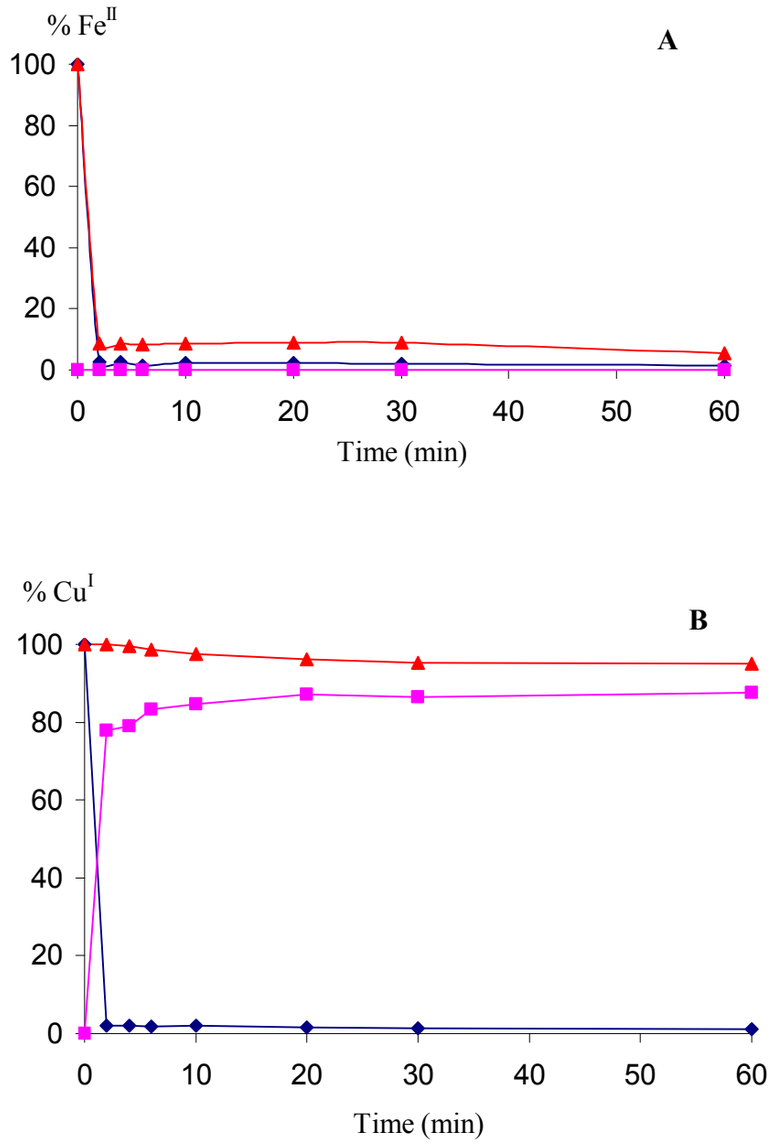

Fig. 3

Food & Function Accepted Manuscript

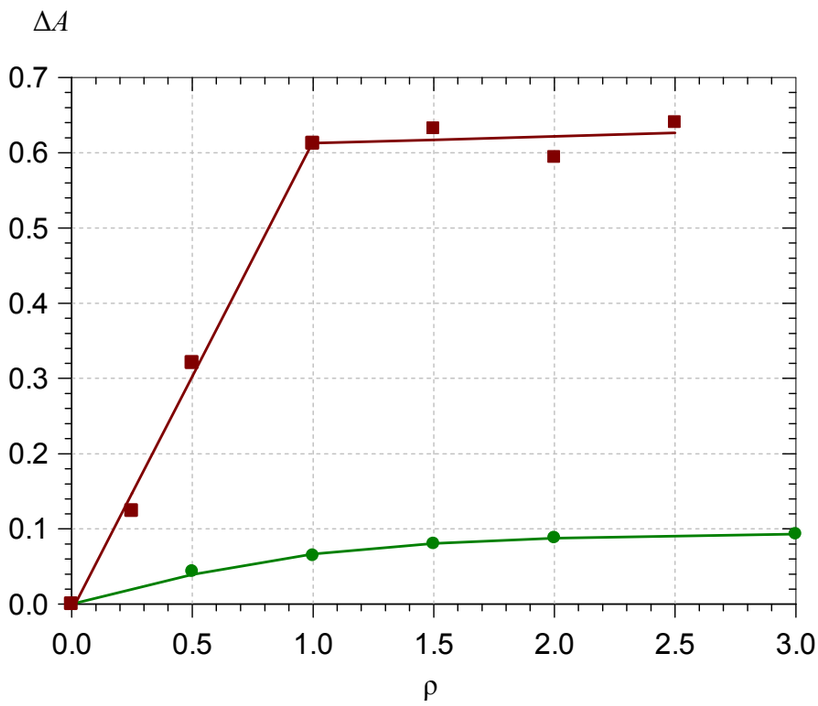

Fig. 4

Food & Function Accepted Manuscript

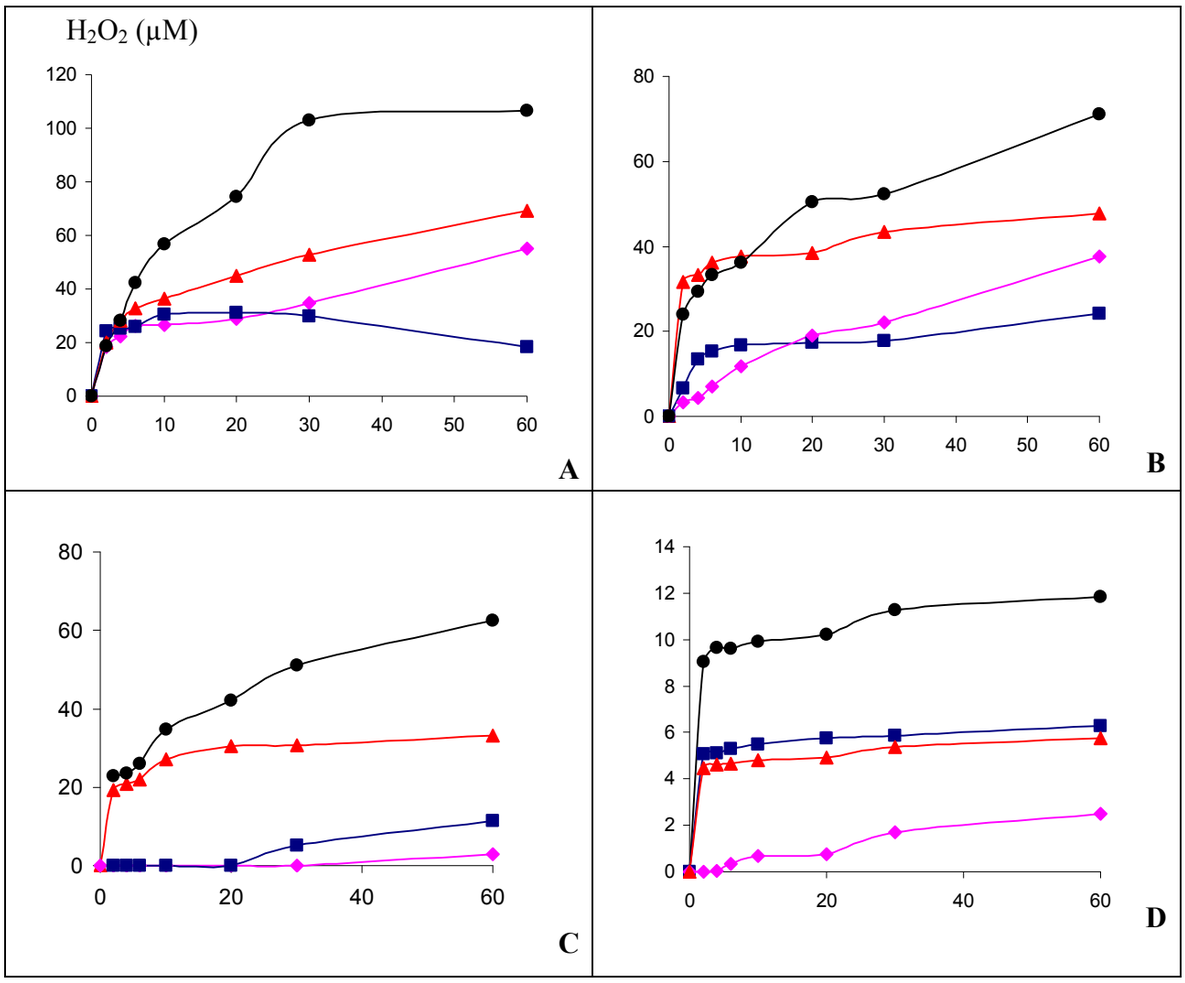

Fig. 5

Food & Function Accepted Manuscript

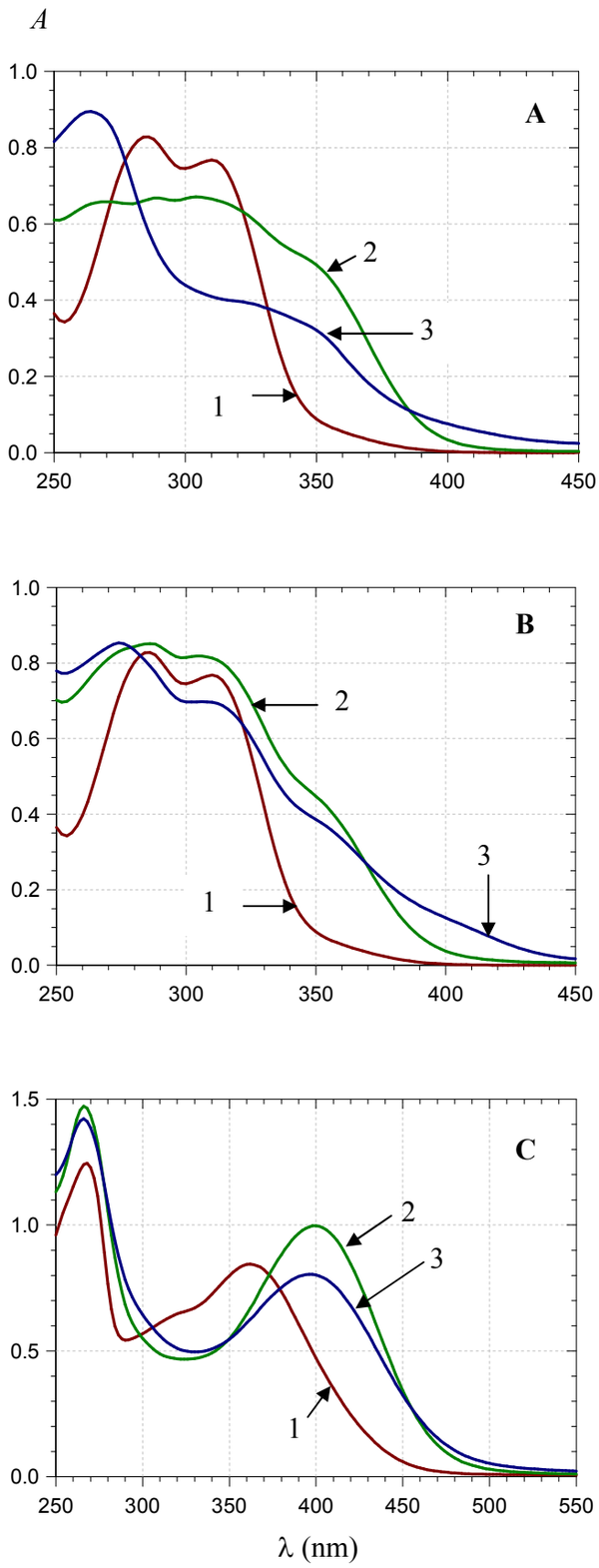

Fig. 6

Food & Function Accepted Manuscript

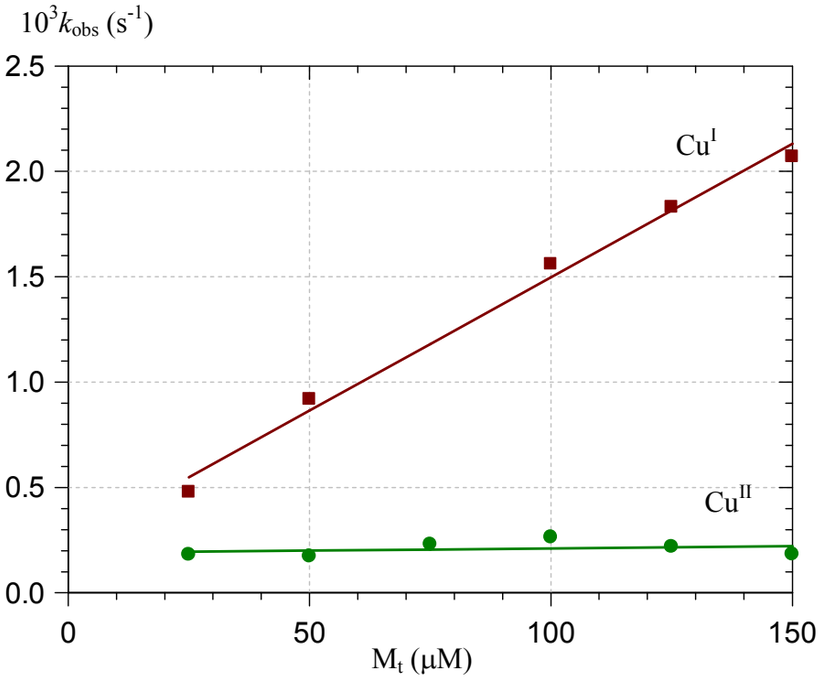

Fig. 7

Food & Function Accepted Manuscript

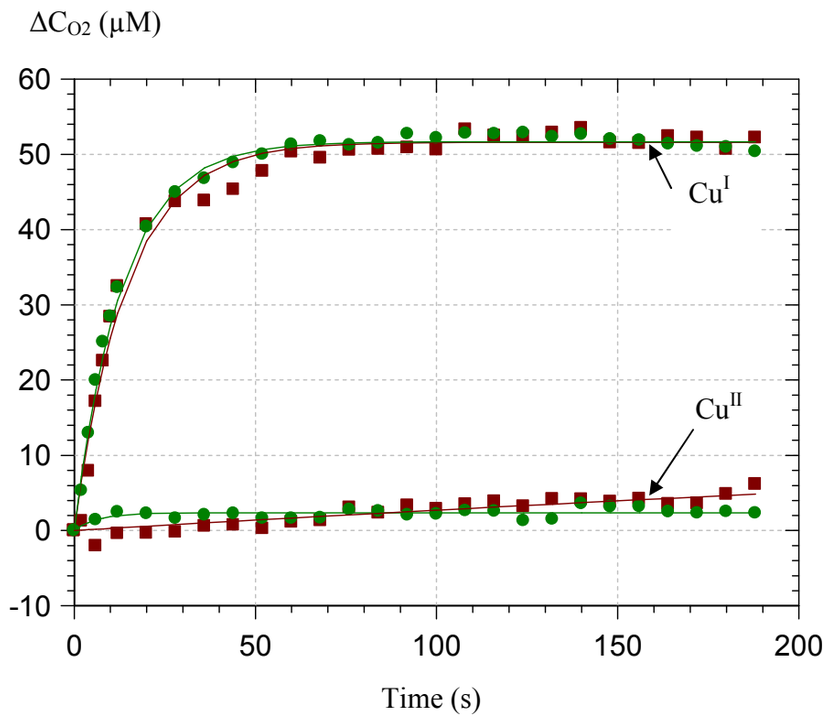

Fig. 8

Food & Function Accepted Manuscript

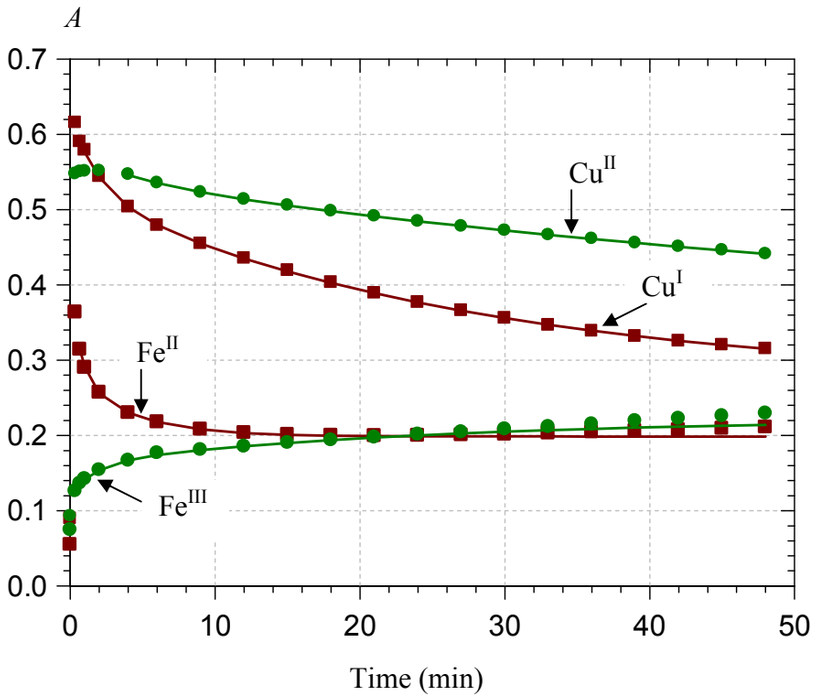

Fig. 9

Food & Function Accepted Manuscript

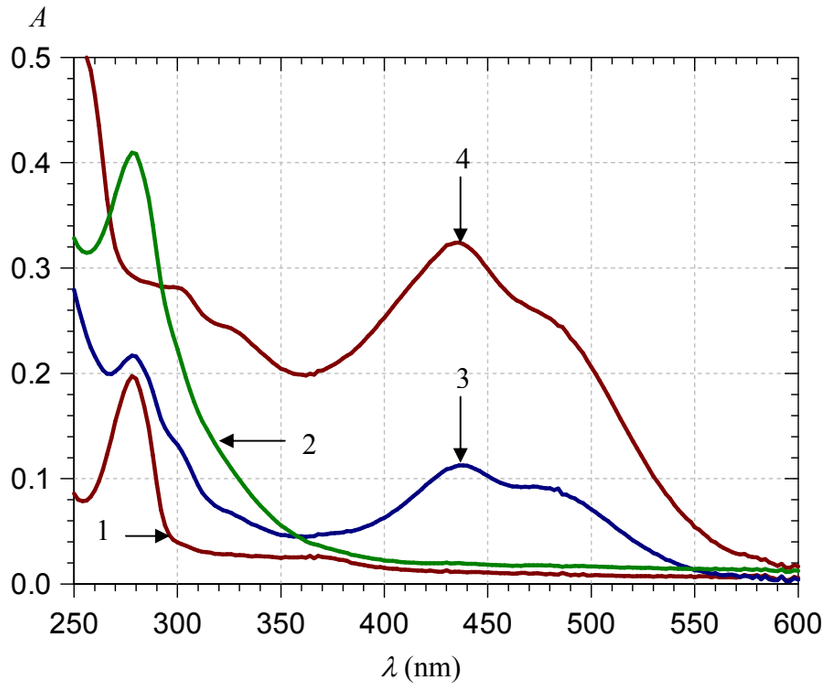

Fig. 10

Food & Function Accepted Manuscript

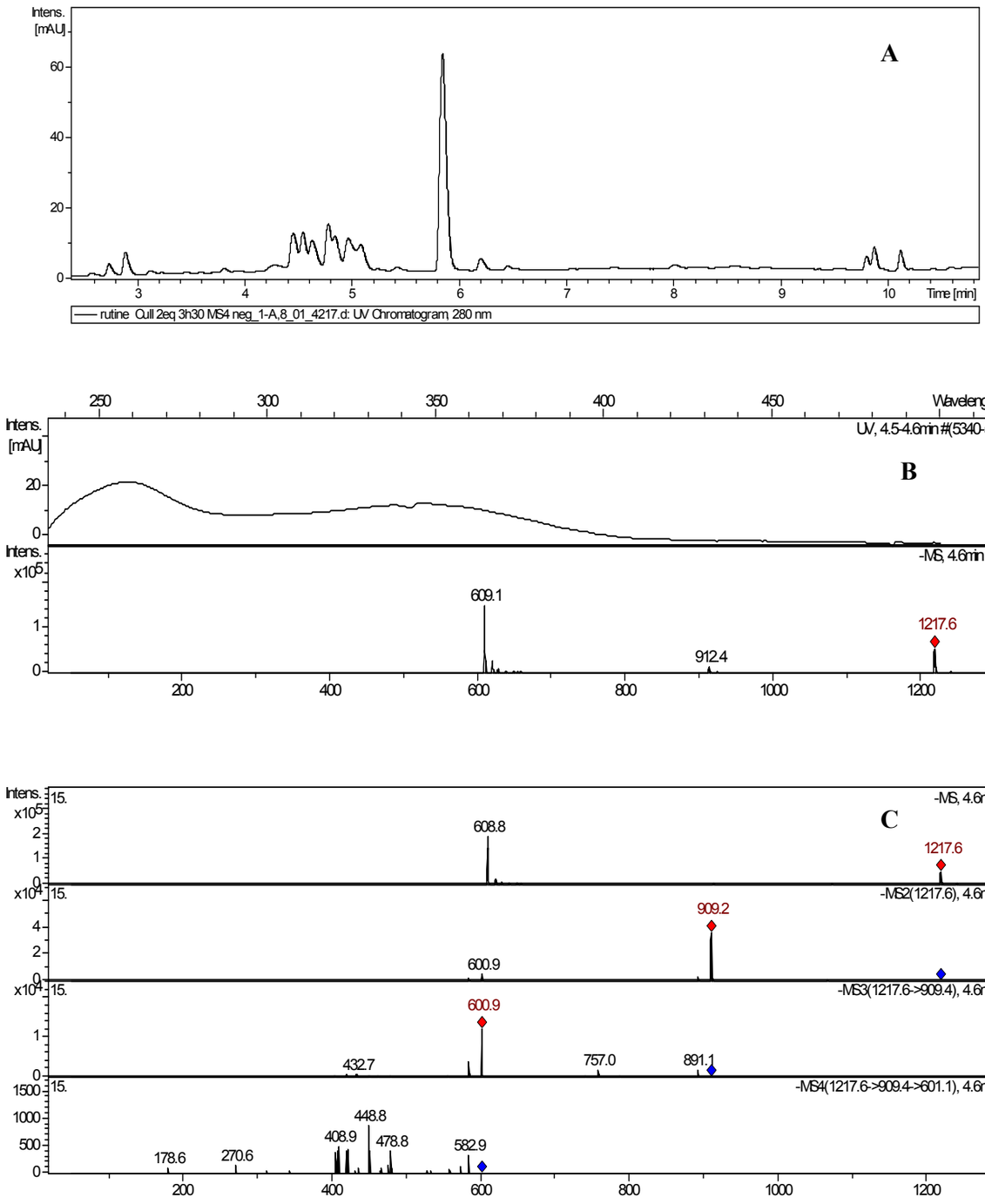

Fig. 11

Food & Function Accepted Manuscript

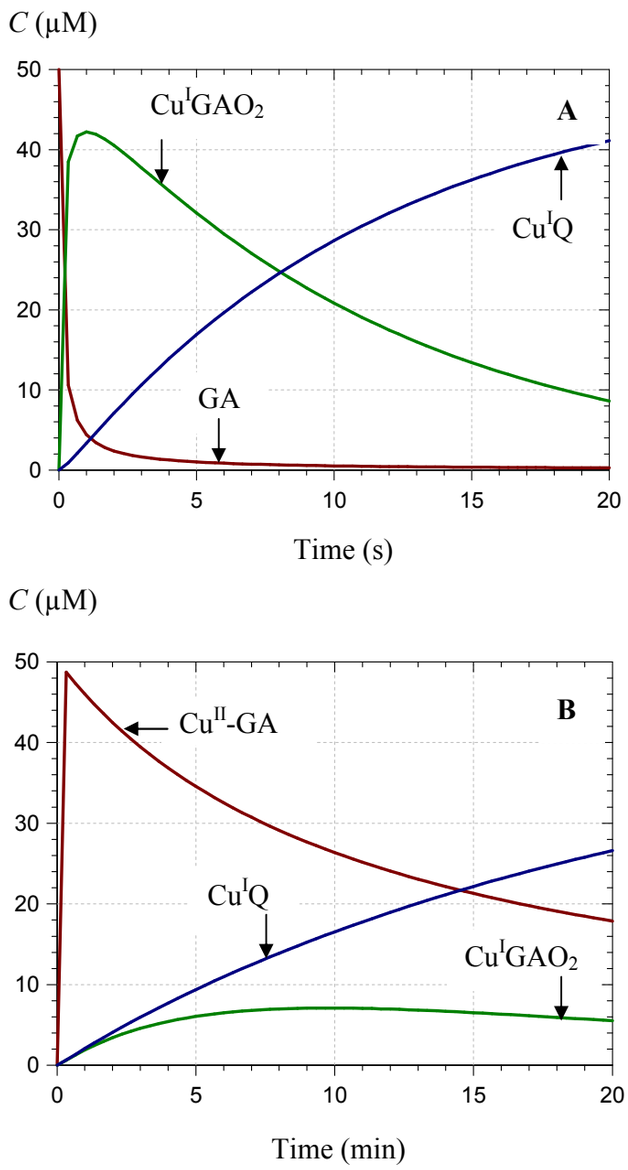

Fig. 12

Food & Function Accepted Manuscript

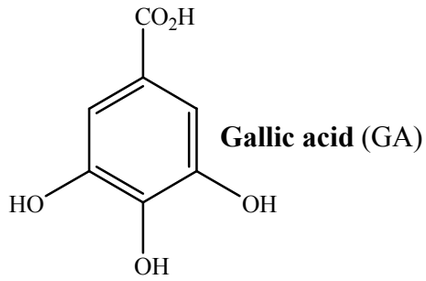

Gallic acid (GA)

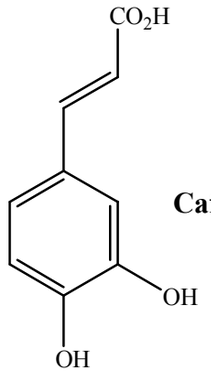

Caffeic acid (CA)

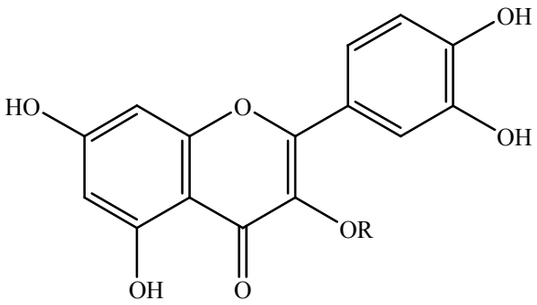

Rutin (R = β-D-Glc-1,6-α-L-Rha)

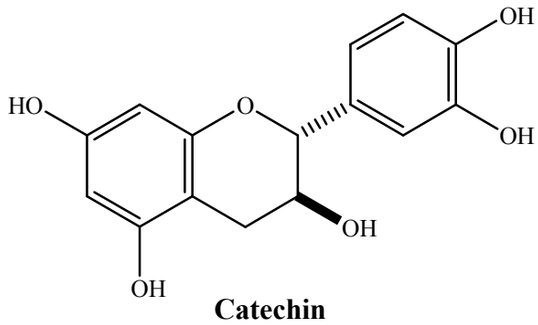

Catechin

Scheme 1

Food & Function Accepted Manuscript

$$Cu^{I} + O_2 \underset{k_{-1}}{\overset{k_1}{\rightleftharpoons}} Cu^{I}O_2$$

$$Cu^{I}O_2 + Cu^{I} \xrightarrow{k_2} 2Cu^{II} + H_2O_2$$

$$Cu^{I}O_2 + GA \xrightarrow{k_3} Cu^{I}GAO_2$$

$$Cu^{I}GAO_2 \xrightarrow{k_4} Cu^{I}Q + H_2O_2$$

Scheme 2

$$Cu^{II} + GA \xrightarrow{k_5} Cu^{II}GA$$

$$2Cu^{II}GA \xrightarrow{k_6} Cu^{I}Q + Cu^{I}GA$$

$$Cu^{I}GA + O_2 \underset{k_{-1b}}{\overset{k_{1b}}{\rightleftharpoons}} Cu^{I}GAO_2$$

Scheme 3

Food & Function Accepted Manuscript

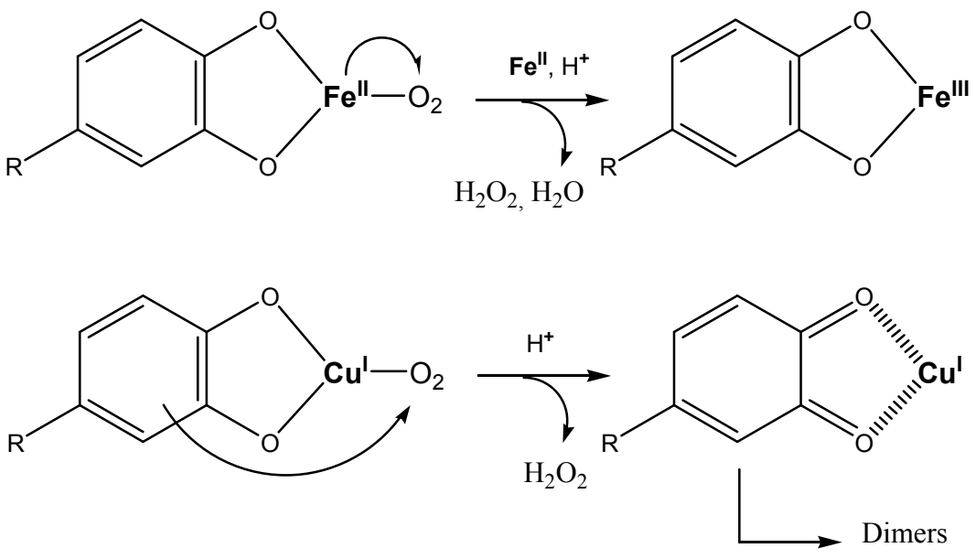

Scheme 4

Food & Function Accepted Manuscript